Physics and Chemistry of the Earth 98 (2017) 136–153

Contents lists available at ScienceDirect

Physics and Chemistry of the Earth

journal homepage: www.elsevier.com/locate/pce

H/V measurements as an effective tool for the reliable detection of landslide slip surfaces: Case studies of Castagnola (La Spezia, Italy) and Roccalbegna (Grosseto, Italy)

Veronica Pazzi*, Luca Tanteri, Gabriele Bicocchi, Michele D'Ambrosio, Andrea Caselli, Riccardo Fanti

Department of Earth Sciences, University of Firenze, Via G. La Pira 4, 50121 Firenze, Italy

ARTICLE INFO

Article history:
Received 16 February 2016
Received in revised form
26 September 2016
Accepted 20 October 2016
Available online 25 October 2016

Keywords:
H/V method
Landslide
Slip surface reconstruction
Model output optimization
GIS
Passive seismic

ABSTRACT

A variety of methods (detailed geomorphological surveys, geotechnical investigations, local instrumentation, satellite data, and radar interferometry) along with geophysical techniques may be used to investigate slope instabilities and to detect the inhomogeneities of materials as well as their properties, boundaries, and sliding surfaces. Of these techniques, the method based on seismic noise measurements allows abrupt changes in seismic impedance at landslide boundaries resulting from varying levels of seismic velocity and material density to be detected. Peaks of the Horizontal to Vertical Spectral Ratio have proven to serve as effective indicators of the resonance frequency of low-impedance surface layers. In this work, horizontal to vertical spectral ratio surveys of the Castagnola (La Spezia, Italy) and Roccalbegna (Grosseto, Italy) landslides were carried out. From roughly 100 single-station measurements made inside and outside the landslides at each site, we define a threshold number of single-station seismic noise measures beyond which information is redundant because the variation in reconstructed impedance contrast surfaces is not significant. This approach allows one to reliably retrieve the geometry of a landslide body, ultimately generating useful information for determining whether further measurements are needed to improve landslide body reconstruction.

1. Introduction

Slope instabilities, which are some of most dangerous phenomena that affect human life and properties, can cause vast direct and indirect socioeconomic losses. Although a reliable way to prevent these damages would involve avoiding the construction of cities near areas that are susceptible to landslides, rapid population growth unfortunately often makes this solution inevitable, resulting in a sort of forced cohabitation. Landslides involve approximately all geological materials and can occur and evolve in a large variety of shapes and volumes (Cruden and Varnes, 1996). Consequently, only an adequate knowledge of these complex phenomena and their kinematics and evolution can help reveal the correct solution. The investigation of deformation processes and landslide characterization is not a simple task and requires access to a broad range of data and observations. Detailed geomorphological surveys, geotechnical investigations, local instrumentation, remote-sensing satellite data, aerial techniques, meteorological parameters analyses, and Synthetic Aperture Radar (SAR) interferometry can be employed (Antolini et al., 2013; Bicocchi et al., 2015, 2016; Fidolini et al., 2015; Frodella et al., 2015; Tofani et al., 2014). Moreover, geophysical techniques can be used to investigate slope instabilities and understand material inhomogeneities and their properties, boundaries and potential slip surfaces (Hack, 2000; Lotti et al., 2015; Maurer et al., 2010).

According to Jongmans and Garambois (2007), geophysical techniques can be used for the subsurface mapping of landslides with both advantages and disadvantages. On the one hand, geophysical methods i) are flexible, relatively efficient and deployable on slopes; ii) are non-invasive and generate information on the internal structures of soil or rock mass; and iii) allow one to examine large volumes of soil. On the other hand, i) resolution decreases with depth and is dependent on the signal-to-noise ratio; ii) the solution for a set of data is non-unique, and the results must be calibrated; and iii) these methods yield indirect information on subsoil such as physical parameters rather than geological or geotechnical properties. Moreover, the success of geophysical methods is mostly dependent on the presence of a significant and

* Corresponding author.
E-mail address: veronica.pazzi@unifi.it (V. Pazzi).

http://dx.doi.org/10.1016/j.pce.2016.10.014

detectable contrast in the physical properties of different lithological units. However, because almost all of the advantages of geophysical methods correspond to disadvantages of geotechnical techniques and vice versa, the two investigation techniques can be considered complementary.

Among all of the geophysical techniques that are available, seismic refraction, reflection, and electrical tomographies are difficult to set up and require the use of complex processing tools, thus causing them to be expensive and time-consuming. Over the last ten years, passive methods based on seismic noise measurements have been used more frequently. Lithology, porosity, and interstitial fluids affect P-wave velocities and, with the exception of interstitial fluid, shear wave (S-wave) velocities. Because slip surfaces can generate shear wave velocity contrasts (landslide mass can be represented as a softened layer wherein changes in seismic impedance at boundaries result from the varying seismic velocity and density of materials) and polarize seismic noise, seismic noise methods can theoretically detect such surfaces (Castellaro et al., 2005; Danneels et al., 2008; Galea et al., 2014; Panzera et al., 2012 and references within). Although this method was originally devised to investigate flat and horizontally layered sites, it also proved capable of revealing resonance properties in more complex settings such as unstable or marginally stable slopes (Del Gaudio et al., 2014).

Nevertheless, seismic noise amplification has rarely been employed as a method to reliably detect landslide slip surfaces (Del Gaudio et al., 2014 and references within), but in the last several years, it has been applied to examine the seismic triggering of landslides. In fact, a layer's geometry (topographic effects) and strong impedance contrasts between seismic bedrock and landslide deposits (local seismic amplification) may be responsible for triggering or reactivating landslides (Bourdeau and Havenith, 2008; Bozzano et al., 2011; references within; Galea et al., 2014; Moisidi et al., 2012, 2015). Seismic noise methods, which require less instrumentation and the use of less sophisticated processing tools, are cost effective, fast and easy to deploy and applicable even to hardly reachable areas (Bonnefoy-Claudet et al., 2006; Delgado et al., 2000; Lermo and Chavez-Garcia, 1994; Méric et al., 2007). These features make the technique useful for other purposes such as seismic site characterization, environmental seismology and seismic vulnerability estimation (Bonnefoy-Claudet et al., 2006; Del Soldato et al., 2016; Galea et al., 2014; Larose et al., 2015; Moisidi et al., 2012; Pazzi et al., 2016a, 2016b).

The present study focuses on the relation between the number of single-station seismic noise measurements employed and resulting inferred slip surfaces for landslides. The aim is to detect, if it is present, a threshold in the number of measurements beyond which information obtained is redundant because the variations observed in the reconstructed impedance contrast surface are no longer significant. To accomplish this objective, i) a seismic noise survey of two selected sites where landslides have occurred was carried out. ii) These data were then analysed to determine the depth of the deepest seismic impedance contrast, which can be associated with a single sliding surface or the envelope of more coalescent surfaces. iii) Punctual measurements of the depth of the sliding surface were then interpolated by means of GIS software to reconstruct the sliding surface. iv) Finally, the number of measurements employed was then reduced step by step, and the resulting sliding surface was compared to the other surfaces obtained, considering the other steps.

The methodology was validated for a site in Castagnola (La Spezia, Italy), for which direct measurements (drillings, piezometers, inclinometers, and InSAR data; Antolini et al., 2013) were available, and it was then applied to another much smaller landslide area for which no direct information was available, i.e., the Roccalbegna landsides (Grosseto, Italy). The resulting surface reliably represents the interface between materials involved in the landslides and underlying undisturbed layers (seismic bedrock), i.e., the sliding surfaces.

2. Study areas

2.1. Geological background

The Northern Apennine is a NE-verging fold-and-thrust belt whose origin is related to the closure of the Jurassic “Ligure-Piemontese” Ocean, which started in the Cretaceous, and to a subsequent Oligocene-Miocene collision between the Corso-Sardinian block and Adria microplate (e.g., Boccaletti and Guazzone, 1974). In this structural asset, two main palaeogeographic domains are identifiable: the oceanic Ligurian Basin and the Continental Adriatic Margin. The Ligurian Units are the most elevated in the nappe pile and consist of Jurassic ophiolites (representing the remains of the Ligurian oceanic crust), and their sedimentary cover of pelagic deposits and flysch units spans in age from the Upper Cretaceous to the Eocene. During accretion, these units formed an accretionary wedge that was overthrusted from west to east, and Umbro-Tuscan units then deposited on the western continental margin of Adria (Abbate et al., 1980). These Umbro-Tuscan units include (from bottom to top) a thick Triassic evaporitic sequence and a Mesozoic sedimentary sequence of a carbonatic platform followed by sediments of pelagic environments and thick siliciclastic turbiditic sequences. The Subligurian Units are tectonically sandwiched between the Ligurian and Umbro-Tuscan units, and they are thus generally referred to as a paleogeographic domain positioned between the oceanic Ligurian Basin and Continental Adriatic Margin (e.g., Bortolotti et al., 2001). From the Oligocene to the present, the Northern Apennines have experienced two phases of eastward migrating deformation: early compression with eastward thrusting and a subsequent phase of extension (e.g., Elter et al., 1975). Tectonic activity related to these deformation phases caused the opening of several NW-SE trending basins, which were subsequently filled with sediments eroded from sedimentary rocks forming the mountain chain.

2.2. Castagnola and Roccalbegna landslides

The Castagnola landslide (hereafter the CL), located in the province of La Spezia, covers roughly 540,000 m^2 and has an approximate volume of 6,000,000 m^3 (Fig. 1a). The CL is a well-known landslide since the late XII century, having caused frequent damage to the surrounding buildings and church of the Castagnola Village (Lagormarsino, 2002). The first investigations carried out in this area date to the early 1970s and were initially limited to surveys focused on geological mapping (Decandia and Elter, 1972). In the second half of the 1980s, the first in-depth geological surveys designed to assess hydrological risks in the national territory (including the CL) were undertaken by the national group for the defence of natural disasters (GNDCN). According to Nosengo (1987), the CL originated from complex roto-translational movements involving both soils and bedrock. The latter consists of Ligurian Units ophiolitic, sedimentary series outcrops and intensely altered limestone blocks interbedded with shale (“Argille a Palombini” Fm.) and mafic intrusive rocks (serpentine and gabbro) of a former oceanic crust. In addition, outcrops of cherts (“Diaspri di Monte Alpe”; Fig. 1a) exist at the southeastern margin of the area. In February of 2001, an initial

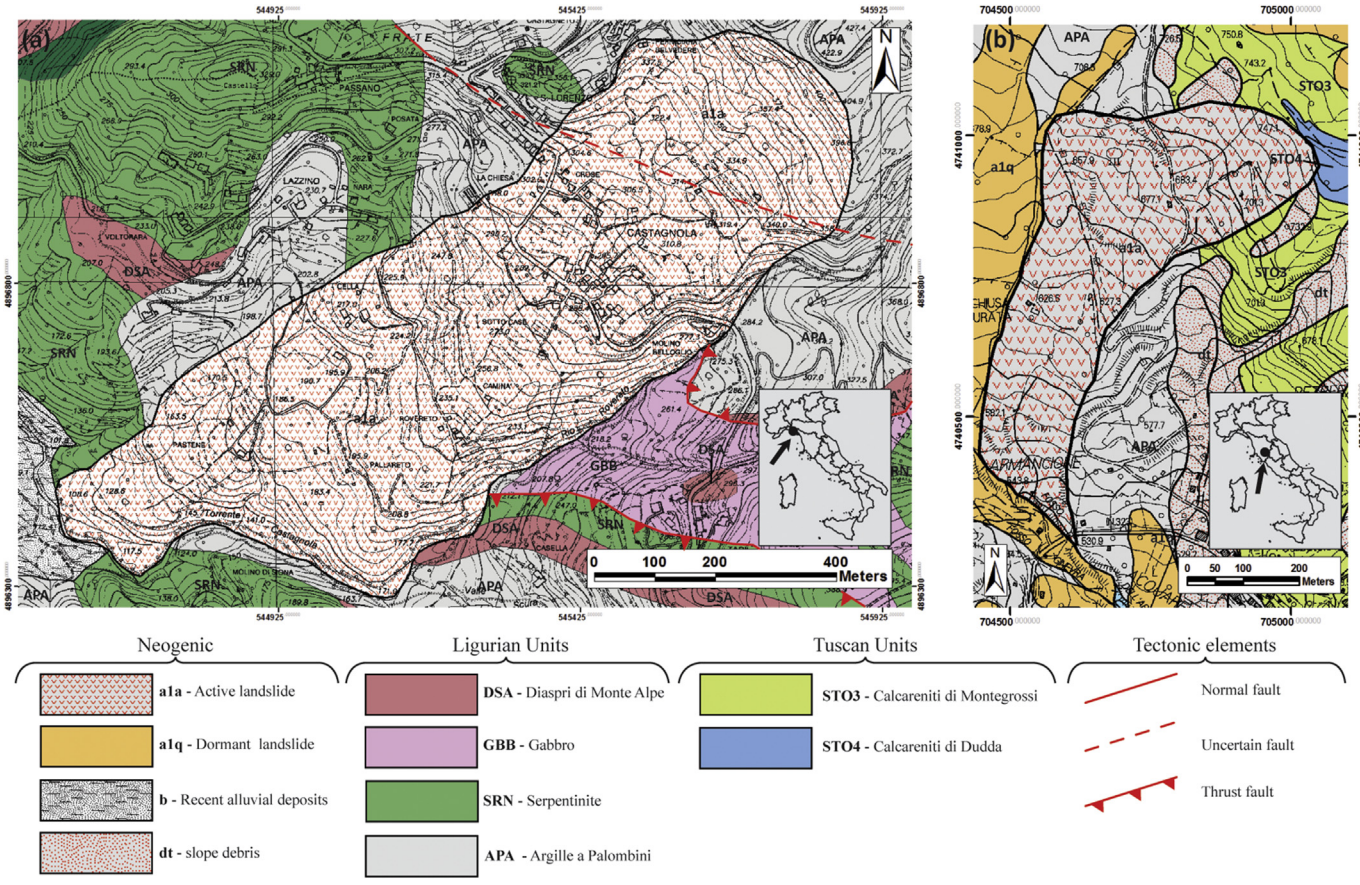

Fig. 1. Maps of geological units and formations in the two test sites: (a) Castagnola landslide (CL) and (b) Roccalbegna landslide (RL). The CTR (Regional Technical Cartography) 1:10,000 topographic basis is available from regional websites.

account of the perimeter of the landslide was included in the national inventory database of landslides. Now, the landslide is monitored by an integrated network of piezometric, pluviometric and radar-interferometric sensors. It is a rather complex landslide with an average displacement rate of roughly 20 mm/yr but is characterized by different areas and layers with various velocities and deformation patterns, complicating the precise reconstruction of sliding mechanisms.

The second test site in Roccalbegna (Grosseto, Italy; Fig. 1b) is an area affected by a roto-translational slide that subsequently turned into an earth flow in its lower portion on February 14, 2014. The Roccalbegna landslide (hereafter the RL) has an extent of roughly 200,000 m^2 and a volume of roughly 2,000,000 m^3 and is located in an area that was previously recognized as an active landslide area (Fig. 1b). The RL includes both Tuscan ("Calcareniti di Dudda" and "Calcareniti di Montegrossi" Fms, consisting of turbiditic limestone block interbedded with thin layers of marl and shale) and Ligurian Units ("Argille a Palombini" Fm.). In the area, the presence of landslides has been reported on the Geological Map of Italy since Jacobacci et al. (1967) and Cestari et al. (1979). In the site, rainfall infiltration is promoted by the presence of hardly cracked clayey soils at the surface, causing water to accumulate at significant depths and causing an increase in water pressure, triggering instability mechanisms. The movement of this landslide typology is typically slow and occurs during maximum rainfall periods when water content exceeds the liquid limit (W_L) of materials. The landslide was monitored until December 2015 using a ground-based radar interferometric sensor and laser scanner.

3. Analytical methods

3.1. Geotechnical properties determination

The effective internal friction angle ϕ' and the total cohesion value c, which is the sum of the effective cohesion c' and of c_a (apparent cohesion), were obtained for an interval of σ (normal tension) of 20–90 kPa using the BST (Borehole Shear Test; Luttenegger and Hallberg, 1981). BST measurements were carried out at a depth of 0.4 m from the ground surface, where soils are often unsaturated. In these conditions, the pore water pressure u_w is lower than the air pressure u_a, with the difference between the pressure levels (u_a-u_w) denoted by soil matric suction, as measured using a tensiometer. The saturated hydraulic conductivity levels k_s was estimated close (~1 m) to the BST site at a similar depth by means of a constant-head well permeameter Amoozemeter (Amoozegar, 1989). The measurement results were processed using the Glover solution (Philip, 1985). In addition to the on-site measurements made, grain size distributions, Atterberg limits and phase relationships (natural water content, porosity, and dry and natural unit weight γ_d and γ) were determined in the laboratory following ASTM recommendations.

3.2. The H/V technique: theory, measurement, and data analysis

Over the last several years, among all of the geophysical passive methods that are available, the horizontal to vertical spectral ratio (H/V or HVSR) method (Nakamura, 1989) has been widely used owing to its cost and time effectiveness. The technique is based on

the measurement of microtremors or environmental seismic noise, which is characterized by low energy and amplitude levels (Okada, 2003) and which has proven to be one of the most suitable procedures for estimating the fundamental or resonance frequency (f_r) of soft deposits. The technique is thus used to study the spectral ratio between horizontal (H) and vertical (V) components of motion recorded at a single station (Cartiel et al., 2006; Lermo and Chavez-Garcia, 1993), as it is well known that the spectral features and polarization of seismic noise show a strong correlation with site geological settings (Lermo and Chavez-Garcia, 1994). Del Gaudio et al. (2014) presented an overview of this technique.

In a planar-layered stratigraphy with varying levels of impedance contrast (e.g., soft sedimentary or fractured layers of overlying bedrock), resonance results from surface wave entrapment between layers. The f_r of the upper level thus corresponds to the ratio between its average shear wave velocity (V_S) and its thickness (h) as shown in the following equation:

$$f_r = \frac{V_s}{4h} \quad (1)$$

According to Castellaro and Mulargia (2009a), if f_{ri} is the central frequency of the ith peak in the H/V-frequency curve, a natural peak (i.e., a peak corresponding to a possible seismic-stratigraphic level or reflector) is clearly denoted by “eye-shaped” detachment in spectral component curves of horizontal components from the vertical one centred at f_{ri} (SESAME, 2004) and by a H/V curve amplitude of <1 around $2f_{ri}$. In practice, H/V curves show several peaks that are caused by the presence (at considerable depths) of several alternating layers of different lithology rather than by the presence of horizontal stratification in homogeneous layers (Fäh et al., 2001; Field and Jacob, 1993; Herak, 2008; Ibs-Von Seht and Wohlenberg, 1999; Lachet and Bard, 1994; Lermo and Chavez-Garcia, 1993; Nakamura, 1989). Moreover, the amplitude of the average H/V curve is related to the impedance contrast between the layer and lower layers (Moisidi et al., 2012). When the layer depth or its V_S are known, it is possible to reconstruct the seismic stratigraphy and subsurface model, and therefore move from the H/V-frequency domain to the depth-V_S domain (Castellaro and Mulargia, 2009b; Lane et al., 2008).

In the two study areas, single-station seismic noise data were collected by means of five Tromino®, an all-in-one compact 3-directional 24-bit digital tromometer developed by MoHo s.r.l. (maximum portability: 1 dm^3 volume and 1 kg weight). Instrument-soil coupling was obtained using the pin set supplied with these instruments, and thus drilling and cable use were not required. Each acquisition ran for 20–24 min at 256 Hz. These instruments were chosen according to SESAME Project (2004) and Italian Civil Protection guidelines on microtremor measurements owing to i) their ease of use, ii) compact size, and iii) absence of connection cables between geophones, seismographs and dataloggers, considerably reducing noise induced by instrumentation on measures of seismic noise.

Each single-station seismic noise acquisition was analysed and processed using the Grilla® software program (by MoHo s.r.l.), which applies guidelines for processing ambient vibration data according to the H/V technique and SESAME project standards (2004). As an initial approximation, each trace was subdivided into 20 s of non-overlapping windows and each window was: i) analysed to keep the most stationary parts of the signal separate from the transient; ii) fast Fourier transformed (FFT) and iii) smoothed using Konno and Ohmachi's (1998) windows at a width equal to 10% of the central frequency. A directional H/V analysis with an angular step of 10° (Del Gaudio et al., 2008) allowed us to evaluate the directionality of each spectral peak. During this first signal analysis, transients were carefully removed. Later, based on these initial outcomes, some parameters such as the analysis frequency range and smooth-window width were changed to the improve results. Consequently, the single component spectra (NS, EW and Z) are the averages computed for all analysis windows, and the final H/V curve is the ratio between the Euclidean average of the horizontal (EW and NS) and vertical (Z) component for each window (Castellaro and Mulargia, 2009a).

In addition, a local seismic stratigraphy model was reconstructed using the Grilla® software: all geotechnical parameters (soil density and porosity) of both sites were derived from the in-situ and laboratory analyses (see § 3.1), and all H/V curves were constrained in terms of velocity. This velocity was estimated by means of direct measures carried out using Trominos: the shot point was located 1 m away from the Tromino such that the velocity in m/s was the reciprocal of the time of the first arrival read on the recorded trace. This procedure was validated for the CL by comparing the calculated velocities with the i) ranges available in the literature; ii) MASW results (Imposa et al., 2015 and references within) and by iii) comparing the thickness of the theoretical model with the results of some inclinometers and stratigraphical logs, as some boreholes/inclinometers were created in 2011 within the landslide's perimeter (Antolini et al., 2013).

Finally, according to Amorosi et al. (2008) and Spizzichino et al. (2013), some alignments crossing the two landslides were individuated, and single-station seismic noise acquisitions acquired along each alignment were elaborated using a tool developed by Castellaro to generate synthetic contour maps of the H/V.

3.3. Reconstruction of the deepest impedance contrast surface

For each landslide area, a dataset of single-station measures of the deepest impedance contrast surface value z obtained through seismic stratigraphy inversion (h in Eq. (1)) and resulting from the same discontinuity was created as a geographic reference file (*shapefile* format). Subsequently, the selected depth values derived from timely measurements were applied in a GIS environment and spatially interpolated using the Inverse Distance Weighted (IDW) method (Shepard, 1968). The IDW deterministic method was preferred over other methods such as the kriging method (Oliver, 1990) because it involves the use of very few parameters (a search neighbourhood, an optimized power value, and a minimum number of points). This latter consideration is important because during a second stage, the interpolation was iterated with the same standardized parameters in multiple stages, with each considering a new subset of data with five fewer points than the previous ones. The aim of this step-by-step procedure was to study differences between the resulting reconstructed slip surfaces when reducing the original size of the dataset. This process, as applied to the CL and RL, is summarized in the flowchart shown in Fig. 2.

The IDW method was set up using an elliptic neighbourhood with semiaxes of 200 m × 400 m while considering at least 12 points up to a maximum of 15 for Castagnola and with semiaxes of 60 m × 90 m while considering at least 5 points up to a maximum of 15 for Roccalbegna. To prevent the generation of artefacts from the interpolation, the resulting raster was filtered based on mean values calculated in a circular neighbourhood with a radius length opportunely calculated. Eventually, to establish a more suitable radius length for the filtering neighbourhood, the distance (in meters) between each possible point couple of the dataset was calculated. The radius length was selected as the average value of the 10th percentile of the ordered distribution. Thus, all of the generated depth maps were compared to assess the differences between interpolating with all of the points or with a reduced number (but with a more homogeneous distribution) of points.

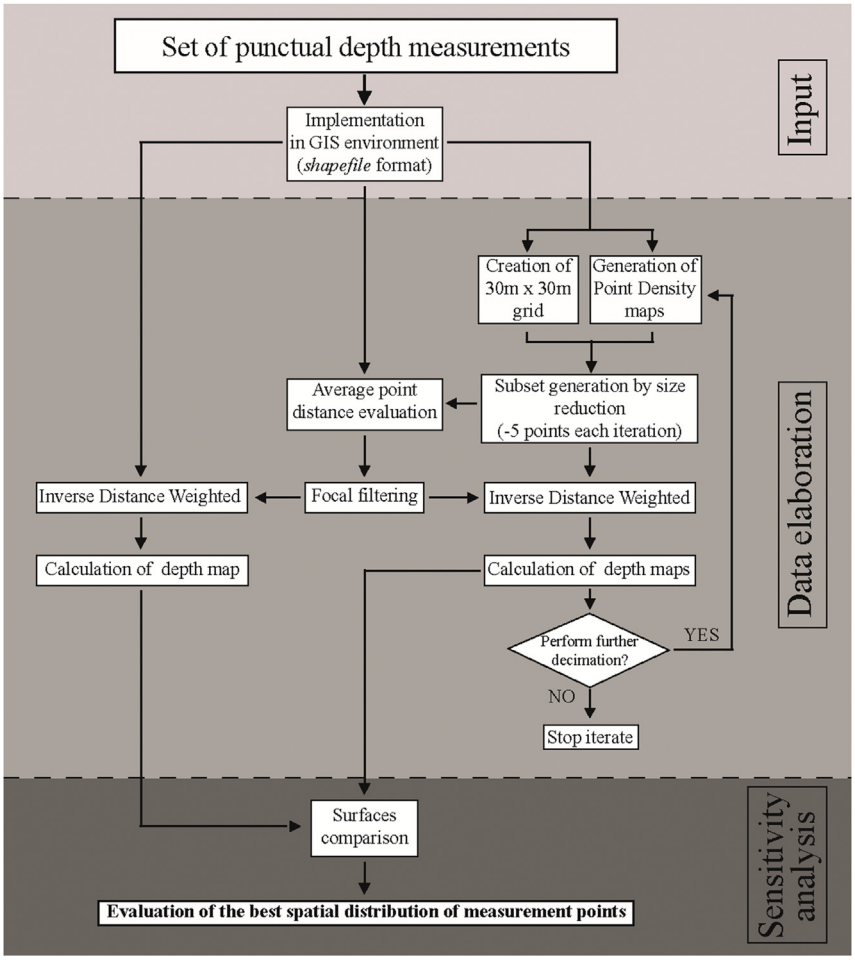

Fig. 2. Flowchart of the reconstruction of the deepest impedance contrast surface.

This comparison was performed using ArcGIS by observing the following:

- internal distributions of depth values in each map (in terms of means and standard deviations);
- volumetric differences between each map;
- geometric differences between reconstructed slip-surface levels for the selected sections.

The main objective was to establish which number and distribution of measurement points is the minimum required to obtain a reliable representation of a level that can be reasonably assumed to be the landslide slip surface or at least an envelope of different contiguous and coalescent slip surfaces.

4. Results

4.1. Geotechnical properties of Roccalbegna and Castagnola

Geotechnical properties of the RL and the CL were identified to characterize shallow layers of materials involved in the landslides. Owing to the rugged terrain in the RL area, on-site investigations were carried out just above the landslide crown, where four different sites (RL-A to RL-D; Fig. 3b) of relatively short extents (10 m) were investigated. For the CL, 3 different sites (CL-A to CL-C; Fig. 3a) in the area covered by the landslide were investigated. In Roccalbegna, although the sand fraction always predominated (from 36.2% to 56.9%) over other fractions in all four samples, grain size distributions were found to vary, and especially in regards to clay fraction abundances (from 8.8% to 20.9%). Furthermore, measured saturated hydraulic conductivity levels were quite variable, ranging from $5\cdot10^{-7}$ to $3\cdot10^{-6}$ m/s. Conversely, the friction angles, dry unit weights and bulk porosities were found to be quite homogeneous among the different samples and were valued at approximately 32°, 16.5 kN m^{-3} and 36.5%, respectively.

In Castagnola, the grain size distributions were found to be characterized by high volumes of sand (up to 46.1%) and gravel (up to 34.3%). The saturated hydraulic conductivity levels, similar to that of Roccalbegna, covered over one order of magnitude (from $4\cdot10^{-7}$ to $1\cdot10^{-6}$ m/s). The dry weight unit was recorded as 15.5–18.1 kN m^{-3}, with higher values corresponding to the gravel-rich CL-B sample. Owing the Atterberg limits of the Roccalbegna and Castagnola samples, W_L varied from 28% to 35% and from 36% to 39%, respectively, while W_P ranged from 20% to 26% and from 28% to 30%, respectively, thus reflecting slightly plastic behaviour in both cases (IP from 7% to 9%). These results are summarized in Table 1.

4.2. H/V results

The distribution of the seismic noise single-station measures is shown in Fig. 3a and b and is summarized in Table 2. In the CL, 109 acquisitions (94 inside and 15 outside the landslide boundaries) were carried out, and in the RL, 140 acquisitions (118 inside and 22

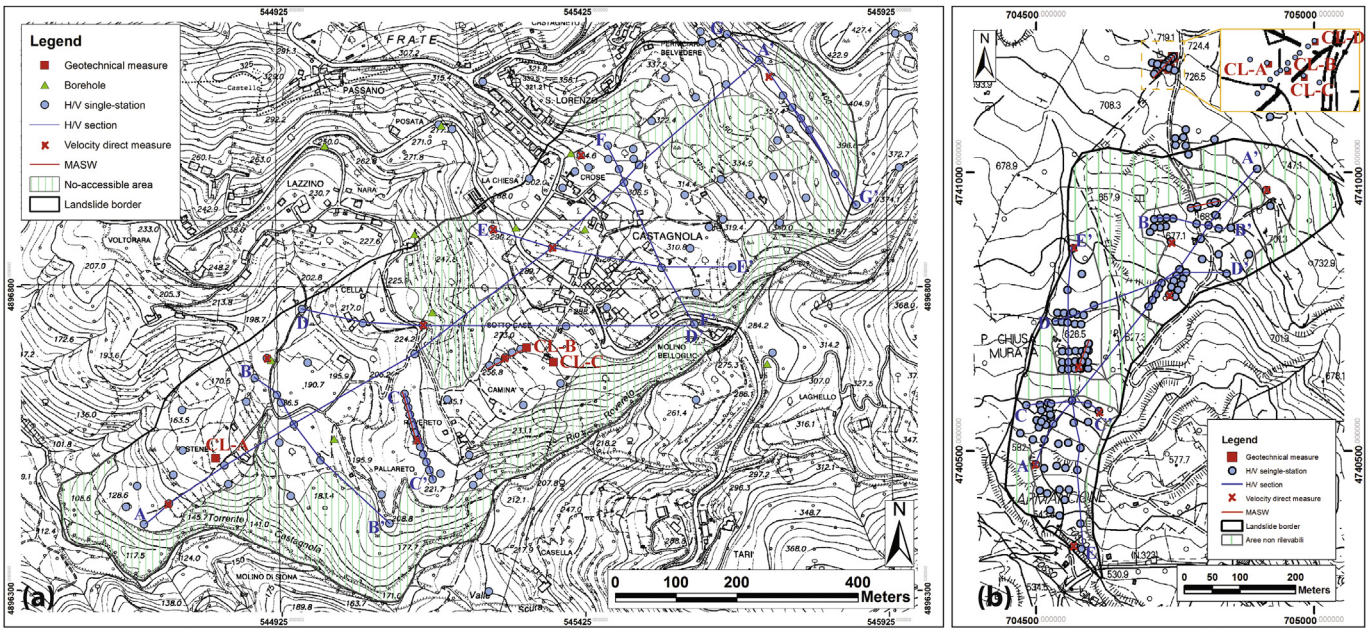

Fig. 3. The spatial distribution of all of the measures (available and performed for the purposes of this work) in (a) CL and (b) RL. Red squares denote geotechnical measures; blue dots denote the H/V station; blue lines denote alignments carried out to produce contour maps of H/V variations; red crosses denote direct measures of velocity; red lines denote the MASW; and striped green areas denote inaccessible areas. Among measures available in the CL, only boreholes (green triangles) are shown. (For interpretation of the references to colour in this figure legend, the reader is referred to the web version of this article.)

Table 1
Geotechnical parameter of Roccalbegna (RL) and Castagnola (CL) soils; the locations of the sites (A to D for Roccalbegna and A to C for Castagnola) are reported in Fig. 3a and b; φ' = effective friction angle, c = cohesion, k_s = saturated permeability, w_n = natural water content, γ = natural unit weight, γ_d = dry unit weight, W_L = liquid limit, W_P = plastic limit, IP = plasticity index, and n.a. = not available.

Site	Gravel (%)	Sand (%)	Silt (%)	Clay (%)	USCS	φ' (°)	c (kPa)	Matric suction (u_a-u_w, kPa)	k_s ($m \cdot sec^{-1}$)	w_n (%)	γ ($kN \cdot m^3$)	γ_d ($kN \cdot m^3$)	Bulk porosity (%)	W_L (%)	W_P (%)	IP (%)
RL-A	26.9	45.5	17.7	9.9	SC	31	2	11.5	5.E-07	18.6	19.3	16.3	37.5	28	20	8
RL-B	10.3	36.2	32.6	20.9	ML	31	2	12.0	3.E-06	16.9	19.3	16.5	36.6	35	26	9
RL-C	14.3	52.8	22.3	10.5	SM	33	0	8.8	2.E-06	19.6	20.3	16.8	35.2	31	25	6
RL-D	15.4	56.9	18.9	8.8	SM	35	7	10.0	6.E-07	16.6	n.a.	n.a.	n.a.	33	26	7
CL-A	29.8	34.7	27.1	8.4	SM	n.a.	n.a.	n.a.	4.E-07	21.2	18.7	15.5	40.5	36	28	8
CL-B	34.3	46.1	15.8	3.8	SM	n.a.	n.a.	n.a.	1.E-06	20.6	21.8	18.1	n.a.	39	30	9
CL-C	n.a.	n.a.	n.a.	n.a.	n.a.	n.a.	n.a.	n.a.	n.a.	21.2	19.7	16.2	37.6	n.a.	n.a.	n.a.

Table 2
Castagnola (La Spezia, Italy) and Roccalbegna (Grosseto, Italy) landslide information: volume, total area and inaccessible area for H/V measures and the total number of H/V single station measures and H/V alignments.

	Castagnola (SP)	Roccalbegna (GR)
Area (m^2)	545,170	191,500
n° H/V single-station measures	109	140
H/V measurements density (points/km^2)	172	217
n° H/V alignment	7	5
No-accessible area (%)	36	50

outside) were carried out. In this figure, green areas denote areas that are inaccessible due to the declivity or presence of brambles and/or dense undergrowth. This area covers roughly 36% of the CL and roughly 50% of the RL. Because it is not possible to list all of the acquired traces here, we list these measures as clustered in Figs. 4 and 5 based on spatial distributions.

4.2.1. Castagnola H/V results

The 94 CL H/V curves, taking into account spatial distributions, can be grouped into 6 main clusters (Fig. 4): in clusters A and B, there is a natural peak at roughly 4–5 Hz (corresponding to a depth of roughly 15–20 m); in clusters C, D and E, there is a natural peak at roughly 3–4 Hz (corresponding to a depth of roughly 20–30 m); and in cluster F, there is a natural peak at 5–6 Hz (corresponding to a depth of roughly 5–12 m). Some of the peaks at higher frequencies visible in all of the clusters are both natural and anthropic. The H/V curves taken from Castagnola are noisier due to the presence of anthropic activity, and natural peaks are often overlaid on anthropic peaks.

4.2.2. Roccalbegna H/V results

The 118 RL H/V curves, considering the spatial distributions, can be grouped into 6 main clusters: in three of them, there is only one natural peak ranging from 3 to 6 Hz (cluster A peak at 4–6 Hz, cluster D peak at 3–5 Hz and cluster F peak at 5–6 Hz corresponding to a depth of 15–40 m), and in two of them, there are two natural peaks that are very close together (cluster B: 4 Hz and 6–7 Hz and cluster C: 3 Hz and 4–5 Hz). Finally, cluster E is very noisy with wide natural peaks, which is likely due to the presence of rough topography with many discontinuities and counter slopes.

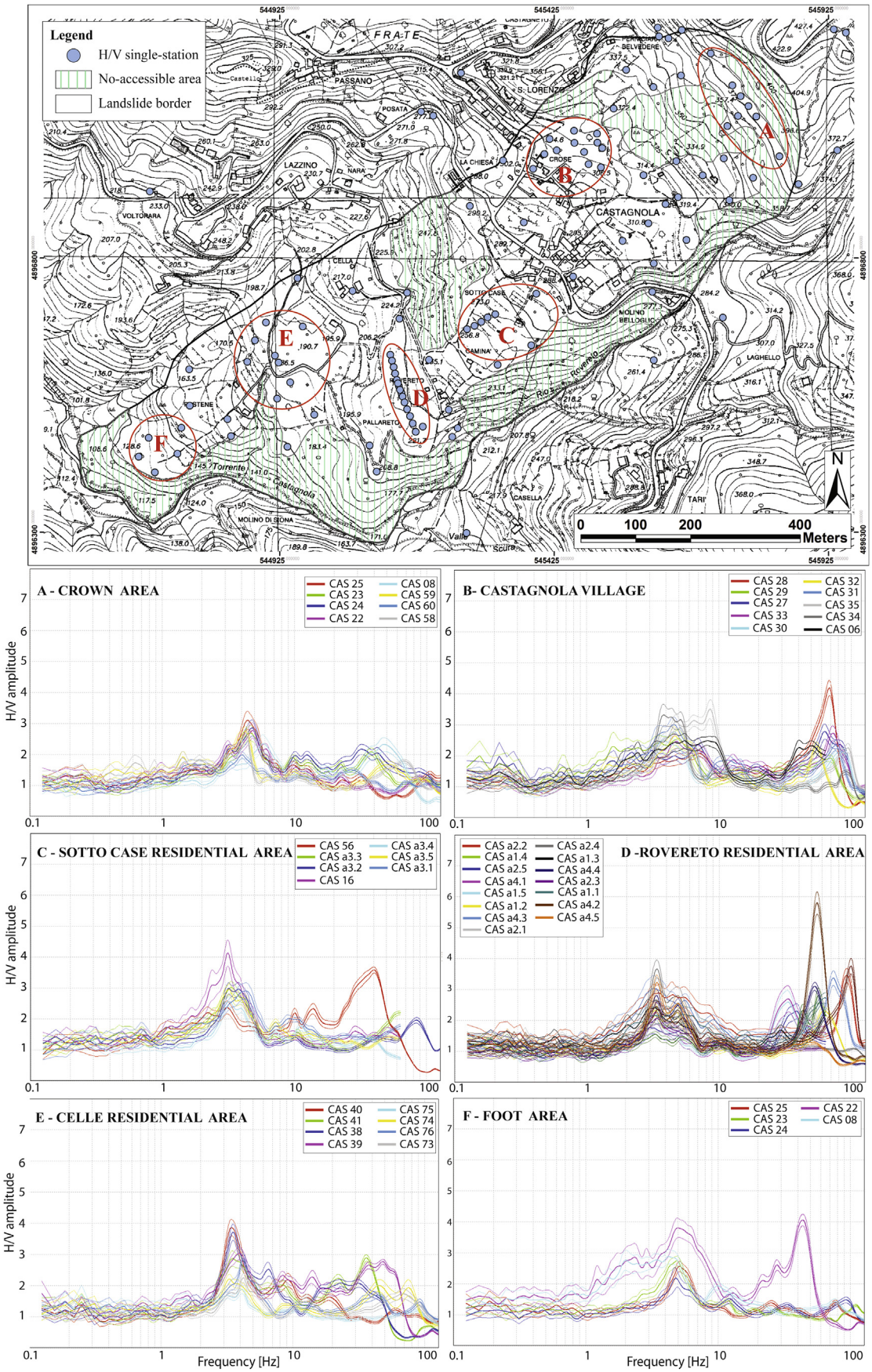

Fig. 4. The CL average H/V curves clustered according to the spatial distribution. Natural peaks occur at roughly 4–5 Hz (clusters A and B), 3–4 Hz (clusters C, D and E) and 5–6 Hz (cluster F).

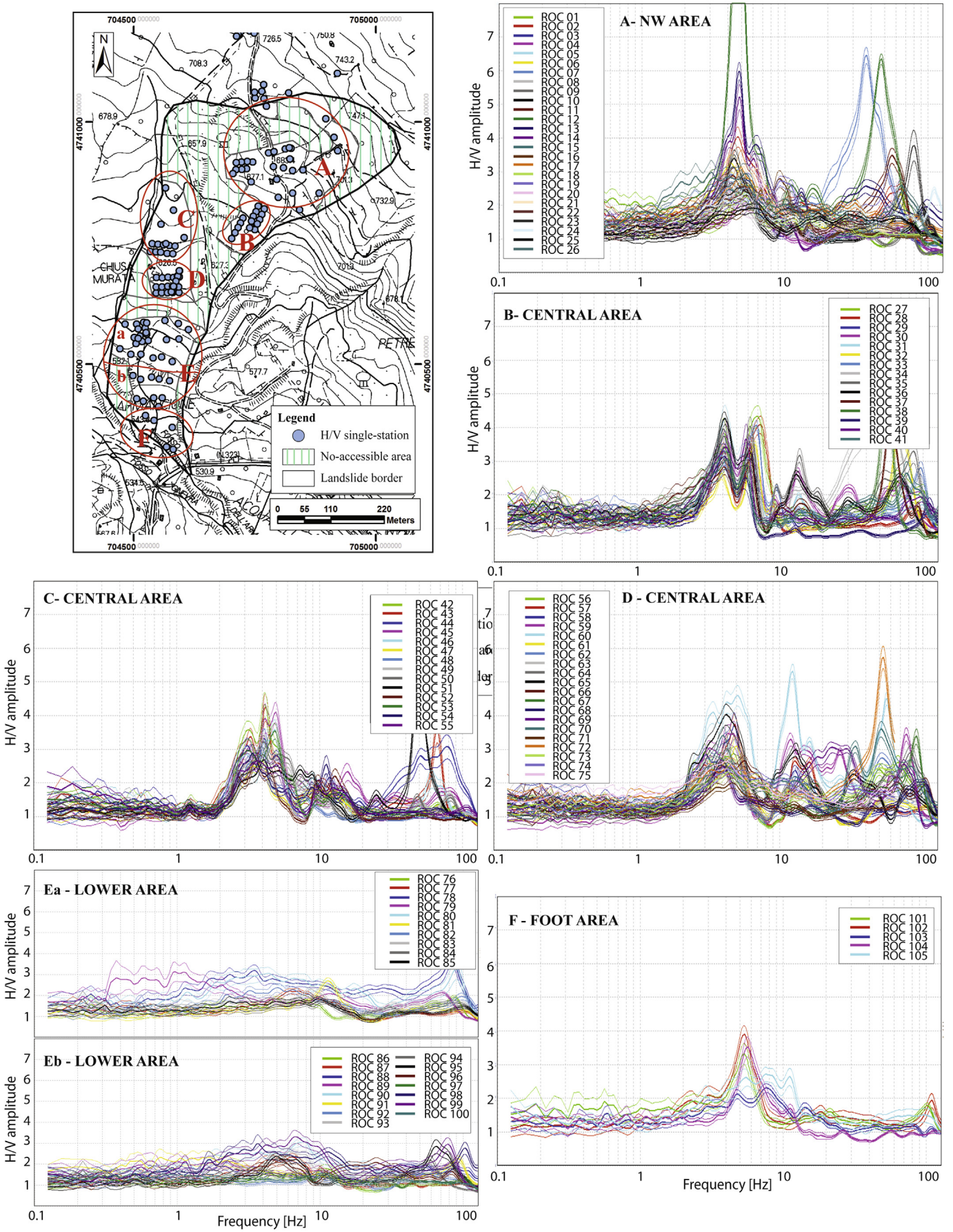

Fig. 5. The RL average H/V curves clustered according to the spatial distribution. Natural peaks occur at approximately 4–6 Hz (cluster A), 3–5 Hz (cluster D), 5–6 Hz (cluster F), 4 Hz and 6–7 Hz (cluster B) and 3 Hz and 4–5 Hz (cluster C). Cluster E (Ea and Eb) is very noisy with broad natural peaks.

4.3. Slip surface depth reconstruction

Punctual depth measurements were collected in a GIS environment and were interpolated using the IDW for the CL and the RL sites to calculate the depth of sub-surface levels hosting the slip surfaces. For each site, the topography of such levels was obtained by subtracting depth maps from the surface topography using a Digital Elevation Model (DEM). The corresponding results are shown in Fig. 6, along with three orthogonal profiles for each site.

Some main features (e.g., volume, mean and maximum depth and surface altitude) inferred from the depth maps of the two landslides are summarized in Table 3. The map of the CL shows a greater depth throughout the village and in the northeastern area and reaches 21.4 m below ground. The depth map for RL shows maximum values in the central part of the landslide body along with a broad area in the northwestern region with a depth nearly equal to zero. This peculiar feature is caused by the total absence of measurement points in this area because it is difficult to access and thus generates locally inaccurate depth reconstructions. Slip surface profiles were generated for each landslide from depth maps and drawn in correspondence with the same sections considered in the seismic data analysis. Table 4 summarizes the main features of the H/V measurement dataset and subsets used for the reconstruction of slip surfaces: the number of H/V measurements, the neighbourhood radius used for filtering and the point density calculated with respect to the landslide area in ha.

The resulting depth maps obtained via the interpolation of single station measurements can serve as reliable representations of the envelopes of landslide slip surfaces. To take this a step further, a general assessment of the accuracy of the resulting depth map and of the method was performed to investigate whether H/V measurements are adequate in terms of quantities, distributions and spatial densities. A grid with 30 m × 30 m cells was created over the landslide perimeter, and cells containing at least one point were selected. Then, the spatial distribution of points was analysed by creating a density map (created using the ESRI® ArcGis 9.3 Kernel Density tool). Five points of the original shapefile were selected from cells with more points in areas with higher Kernel Density values and were then deleted. We in turn produced a reduced dataset with 5 less points than the original one but with a potentially more homogeneous spatial distribution. This subset generation process was repeated, creating a set of shapefiles derived from the original with 5 fewer points relative to that derived from the previous iteration. New raster depth maps were then created using the IDW method and were filtered using a neighbourhood selected based on the average of the 10th percentile of the new point couples of distance distributions for each iteration.

To summarize, from the CL test site, 17 depth maps were generated from 94 points corresponding to a density of 1.72 points/ha using the full dataset and from 14 points corresponding to a density of 0.26 points/ha using shapefiles obtained from the 16th iteration. In the RL test site, 23 depth maps were generated from 118 points corresponding to a density of 6.16 points/ha using the total dataset and from 9 points corresponding to a density of 0.47 points/ha using shapefiles obtained from the 22nd iteration.

5. Discussion

5.1. H/V measurements for reconstructing landslide slip surfaces

Measures carried out in the CL allowed us to fine-tune the proposed methodology. The selection of peaks of interest was validated by comparing the seismic stratigraphic model with data associated with 10 inclinometers placed both inside and outside the landslide perimeter. In particular, our examination of respective inclinometric diagrams reveals pipe ruptures resulting from landslide movements at the same depth as strong impedance contrasts detected using tromometers. The stratigraphical logs obtained by observing drilling cores collected through piezometer installation reveal some intensely deformed levels at variable depths of 10–25 m with clear evidence of underground water circulation within generally undisturbed dry claystone. Sparse centimetric fragments of claystone in a finer plastic and wet matrix have formed such features. Our geotechnical measurements show that within upper soil layers, similar conditions are present. For the collected samples, differences in the abundance of granulometric fractions (i.e., in the grain size distribution) were likely responsible for the variations in saturated permeability and dry unit weight (Table 1). The results of geotechnical surveys performed in the RL can be interpreted the same way, allowing us to hypothesize that variations in grain size distributions are responsible for differences in permeability, whereas for the RL, dry unit weights appear to be less affected than they are in the CL based on grain size distributions. H/V curve data (Fig. 7) and stratigraphic models of the measures performed near four of the boreholes were used to validate the velocity direct measure technique as illustrated in Section 3.2. The depth (h in Eq. (1) and z_{CASi} below) obtained after fitting peaks of the ith H/V curves taken near the inclinometer was found to be comparable to the depth (z_{Sj}) at which jth inclinometers were cut: z_{CAS1} = x m and z_{S07} = 20 m, z_{CAS15} = x m and z_{S08} = 11 m and z_{CAS17} = x m and z_{S10} = 25 m (Fig. 7).

Our analysis of seismic noise records (Figs. 4 and 5) shows that H/V amplification is greater in the RL than in the CL. The CL also does not show significant variations from its central area to its boundaries while in the RL, values decrease from the crow to the foot (Danneels et al., 2008; Delgado et al., 2015). This is likely attributable to mean slope inclination angles of the two landslides (CL: 10° and RL: 13°). Both of these angles are less than 15°, and thus topographic amplification/deamplification effects can be neglected with respect to landslide mass resonance, which is more intense (Bouckovalas and Papadimitriou, 2005; Lenti and Martino, 2012; Wang et al., 2015).

Figs. 8 and 9 present synthetic contour maps of the H/V. In these maps, warm colours (from yellow to red) are associated with positive impedance contrasts ($\log_{10}$ (H/V) > 0), such as a clear contrast between an upper layer of sediment that is more or less saturated or a fractured rock and a deeper layer of intact seismic bedrock (Amorosi et al., 2008). Cool colours (from light to dark blue) are associated with negative impedance contrasts ($\log_{10}$ (H/V) < 0) corresponding to velocity inversion in the uppermost layers (Castellaro and Mulargia, 2009a). Green areas correspond to an absence of impedance contrast and therefore to an absence of seismic velocity variations between layers ($\log_{10}$ (H/V) = 0).

Seven alignments of single-station measures were identified for the CL. For all of these H/V alignments (Fig. 8), it is possible to identify a very high impedance contrast at a mean depth of 30 m associated with the potential sliding surface. Moreover, in section GG′, it is possible to identify lateral landslide boundaries.

Five alignments of H/V measures were identified for the RL. Even for this area, it is possible to identify very high impedance contrasts between all of the sections associated with potential sliding surfaces (Fig. 9). The H/V sections of both sites show a strong correspondence to the profiles obtained by spatially interpolating all timely seismic measurements.

According to Del Gaudio et al. (2014), the use of the H/V technique to detect slip surface depths is mainly based on the principle that the resonance frequency of a landslide can be generated from soft debris (the landslide mass itself) over rigid bedrock, i.e., when low shear-wave velocity layers present a sharp impedance contrast with bedrock. Although this principle is theoretically correct,

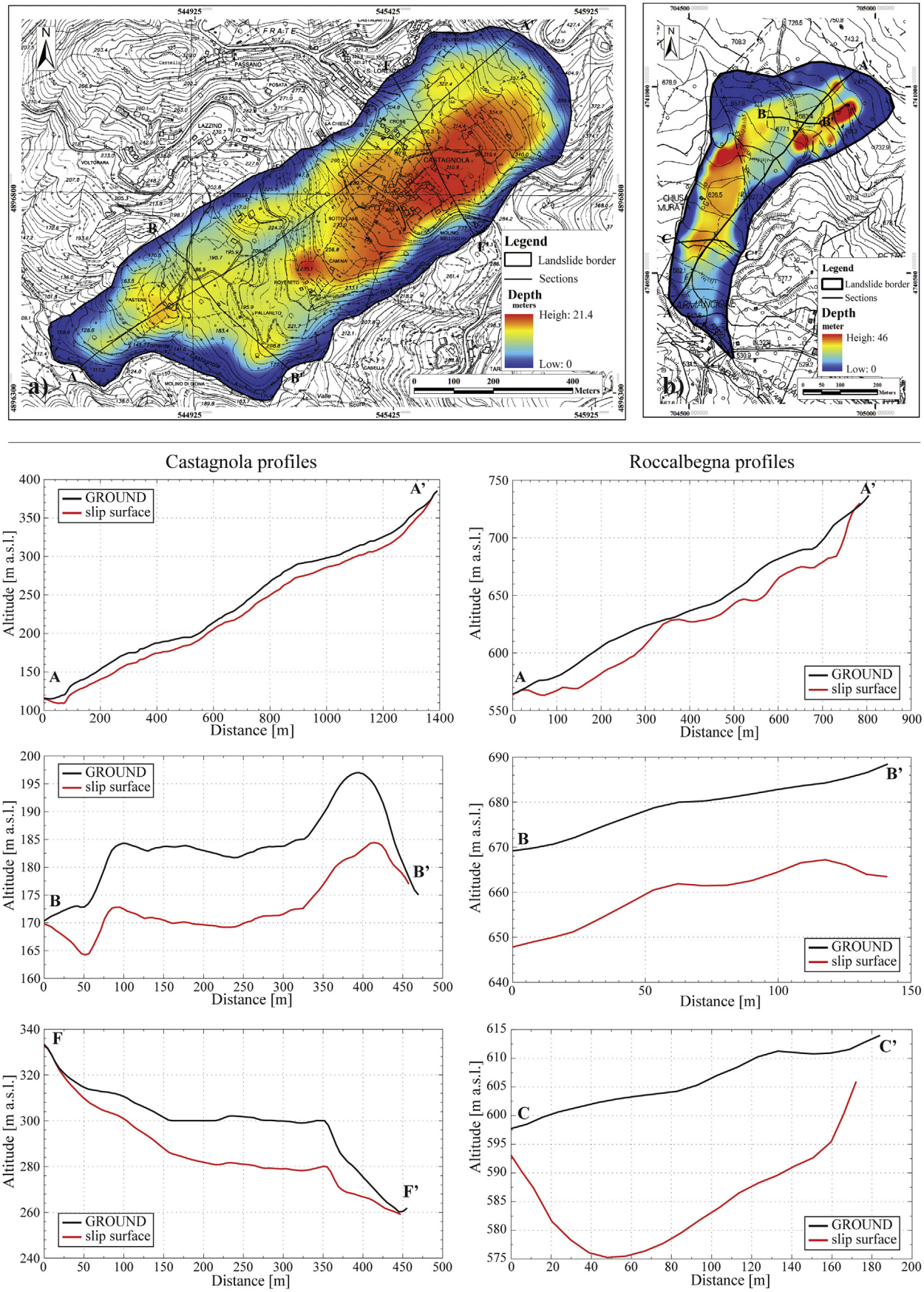

Fig. 6. Slip surface depth maps reconstructed for the CL (a) and RL (b) with sections and corresponding height profiles showing ground and slip surface geometries.

Table 3
Main features of the CL and RL: maximum and minimum heights, volumes, means and maximum depths obtained from the resulting depth maps.

	Castagnola (SP)	Roccalbegna (GR)
Maximum Height (m a.s.l.)	392	750
Minimum Height (m a.s.l.)	245	523
Volume (m^3)	5,843,000	2,220,000
Mean depth (m)	10.7	11.6
Maximum depth (m)	21.4	46.0

several other conditions can spur more complex local seismic responses in landslide masses and thus remove soil resonance effects. Over the last decade, as stated in the introduction, several studies have examined seismic responses in landslide-involved slopes using field evidence, geophysics and numerical modelling. Some of the main outputs obtained thus far have demonstrated that: a) the slope dip can control the expected seismic response of a landslide mass, i.e., in strengthening less-pronounced or absent dip resonance effects; b) depending on the impedance contrast between the landslide mass and bedrock, the main resonance can be measured (or not); c) in the same landslide mass, the impedance contrast can vary from the detachment area to the landslide foot, thus showing that seismic amplification can disappear in parts of a landslide mass; and d) the polarization of seismic noise signals must be considered because this can generate phenomena of resonance directional variability (Galea et al., 2014; Lenti and Martino, 2012; Moisidi et al., 2015; Panzera et al., 2012; Wang et al., 2015).

The geological features and physical properties (i.e., the values of geotechnical parameters) of the two studied landslides and their slope shapes (both have angle slopes less than 15°) justify the reliability of the applied techniques because topographic amplification/deamplification effects can be neglected with respect to landslide mass resonance (Bouckovalas and Papadimitriou, 2005; Lenti and Martino, 2012).

The interpolation workflow iterated by decreasing the number of single H/V stations employed in the determination of slip surfaces allowed us to identify possibly redundant measurements in terms of the quantities and spatial distributions. We in turn determined the minimum number of measures (assuming a homogeneous spatial distribution) that ensure the reliable reconstruction of depths of the investigated level. In doing so, the depth maps obtained for each step were compared in terms of the average depth values and differences in volume for all potential map couples. This latter approach involved comparing a depth raster with a second depth raster by separately calculating the volume of zones where the second one had a greater (volume loss) or smaller depth (volume gain). At this stage, all depth maps were compared to obtain a matrix containing all differences in volume between each couple of surfaces.

5.1.1. Castagnola landslide case study

The results obtained from the Castagnola case study are shown in Fig. 10. The figure presents mean depth values for all 17 maps (Fig. 10a) and differences in volume between the map obtained with all measurements (total map) and the other maps from the 16 iterations (Fig. 10b). Each data series is associated with a regression line determined from a 4th-order polynomial, and trends were analysed by calculating the value of the tangent in relation to the polynomial function of each step. Our analysis of the mean depth plot shows very minor variations for the first nine iterations (dark to light green areas in Fig. 10a). Then, from the 11th iteration onward, the graph shows a considerable increase in gradients, denoting more significant differences between the resulting maps (yellow to red area in Fig. 10a). In particular, mean map depth values corresponding to the first 10 iterations consistently range from 10.79 to 10.67 m with an average value of 10.74 m and a standard deviation of 0.039 m. For the last 5 iterations, values vary considerably to up to 8.73 m due to the insufficient spatial density of measurements.

The series of volume differences between the total depth map and other maps generated from the 16 iterations associated with a regression line and calculated using a 4th-order polynomial is shown in (Fig. 10b). The results show a gradual increase for the zones with volume gains and for the zones showing volume losses within the first 9 iterations, denoting a constant but rather minor

Table 4
Features of the H/V measurement datasets used for the reconstruction of slip surfaces in the CL and RL (TOTAL) and for subsets generated through the iterative process.

	Castagnola (SP)			Roccalbegna (GR)		
	Points	Neighbourhood radius (m)	H/V measurements density (points/ha)	Points	Neighbourhood radius (m)	H/V measurements density (points/ha)
Total	94	35	1.72	118	16	6.16
Iteration 1	89	39	1.63	113	18	5.90
Iteration 2	84	41	1.54	108	19	5.64
Iteration 3	79	42	1.45	103	19	5.38
Iteration 4	74	45	1.36	98	20	5.12
Iteration 5	69	52	1.27	93	21	4.86
Iteration 6	64	48	1.17	88	20	4.60
Iteration 7	59	49	1.08	83	21	4.33
Iteration 8	54	51	0.99	78	21	4.07
Iteration 9	49	52	0.90	73	22	3.81
Iteration 10	44	54	0.81	68	23	3.55
Iteration 11	39	56	0.72	63	26	3.29
Iteration 12	34	60	0.62	58	24	3.03
Iteration 13	29	64	0.53	53	25	2.77
Iteration 14	24	70	0.44	48	27	2.51
Iteration 15	19	75	0.35	43	27	2.25
Iteration 16	14	82	0.26	38	28	1.98
Iteration 17				33	31	1.72
Iteration 18				28	33	1.46
Iteration 19				23	36	1.20
Iteration 20				18	43	0.94
Iteration 21				13	50	0.68
Iteration 22				9	64	0.47

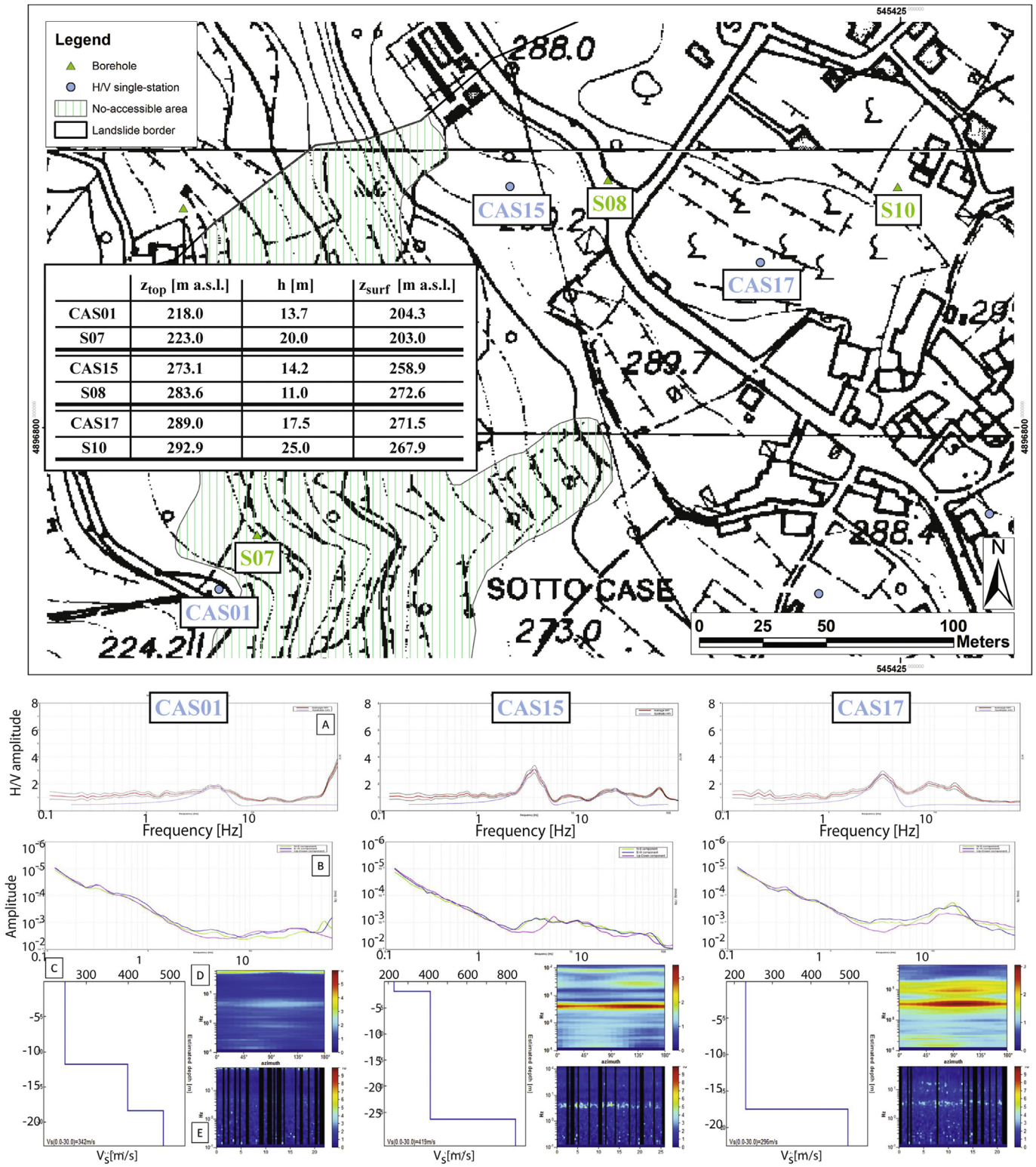

	z_{top} [m a.s.l.]	h [m]	z_{surf} [m a.s.l.]
CAS01	218.0	13.7	204.3
S07	223.0	20.0	203.0
CAS15	273.1	14.2	258.9
S08	283.6	11.0	272.6
CAS17	289.0	17.5	271.5
S10	292.9	25.0	267.9

Fig. 7. Average H/V curves (A), component spectra (B), seismic velocity profiles (C), signal directions (D) and stationary values (E) of the three measures recorded near boreholes. The table summarizes H/V measure and borehole topographic heights (z_{top}), the depths of seismic discontinuities and inclinometer cuts (h) and the topographic height (z_{surf}) of the discontinuity/cut.

increase in differences between the first map and the other maps (green area in Fig. 10b). Within this interval, differences constantly falling below 150,000 m^3 based on the spatial extent of the landslide can be considered very minor (i.e., 2.5% of the estimated total volume). From the 9th and 11th iterations, the two series continue to follow a similar trend but with a slight gradual increase in gradients, whereas from the 11th iteration onward, the two series show completely different behaviour and tend to diverge (yellow

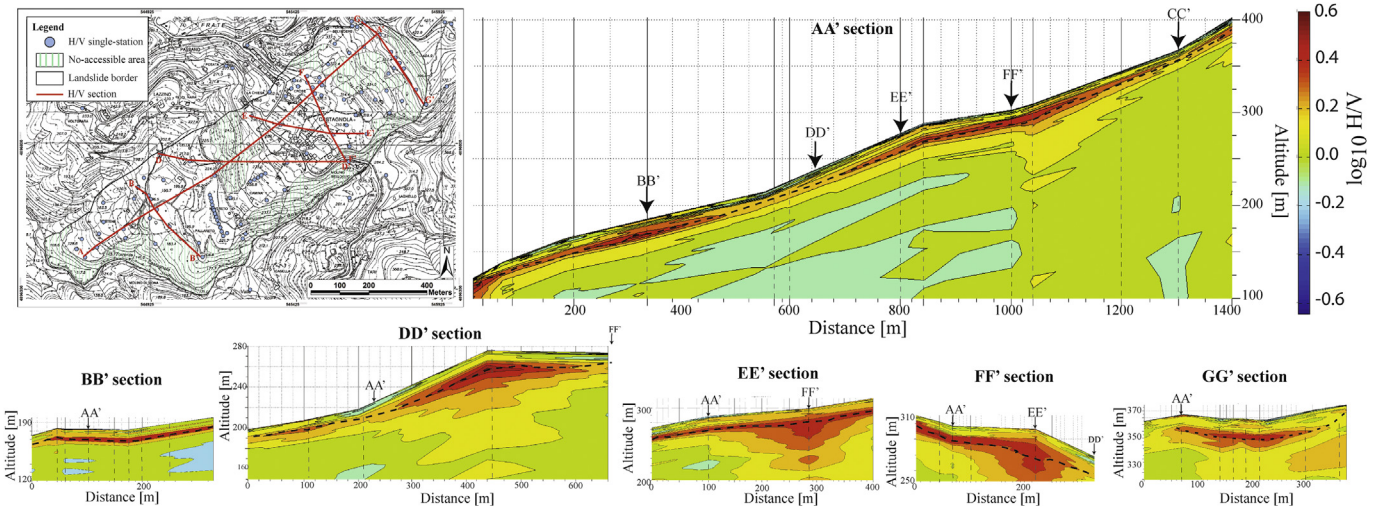

Fig. 8. RL H/V contour maps along the six alignments. Faint vertical dashed lines denote the locations (on the surface) of the H/V measurements. Marked dashed lines denote the main seismic impedance contrast (dark red) associated with the landslide slip surfaces. (For interpretation of the references to colour in this figure legend, the reader is referred to the web version of this article.)

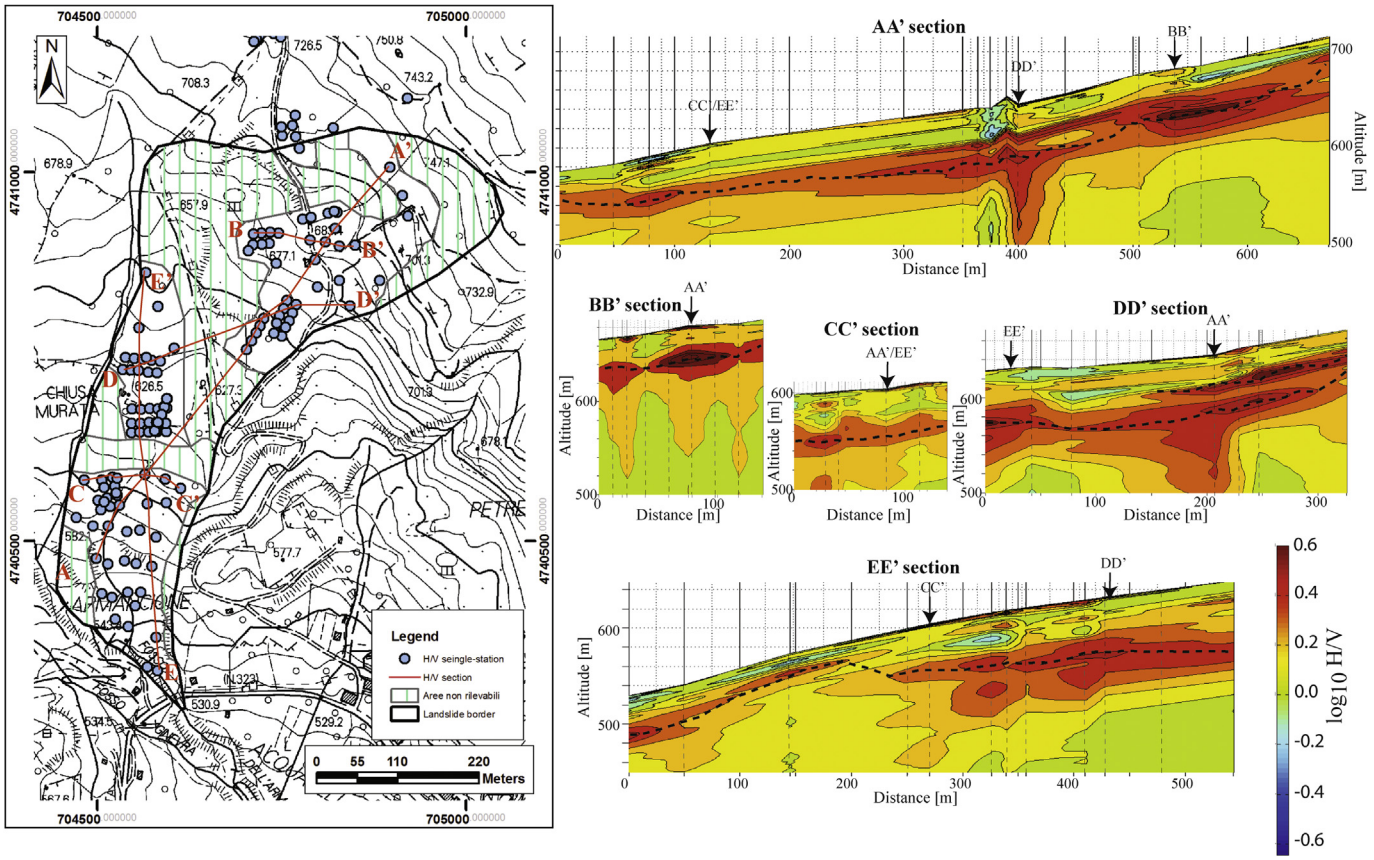

Fig. 9. CL H/V contour maps along the six alignments. Faint vertical dashed lines denote the locations (on the surface) of the H/V measurements. Marked dashed lines denote the main seismic impedance contrast (dark red) associated with the landslide slip surfaces. (For interpretation of the references to colour in this figure legend, the reader is referred to the web version of this article.)

area in Fig. 10b). In particular, the series of volume gain assumes exponential behaviour growth, whereas the differences in volume loss tend to remain constant between the 11th and 14th iterations, beginning to decrease until the last step (red area in Fig. 10b). This can be attributed to the insufficient number and spatial density of measurement points, rendering the calculated surfaces progressively more inaccurate and decreasing in depth.

In Fig. 11a, differences in depth between the map obtained from all of the data and that obtained from data of the 16th iteration are shown with the profiles of sections AA′, BB′ and FF′ (Fig. 11b–d, respectively). These profiles were calculated using depth maps from the total dataset and from the 10th and 16th iterations, and

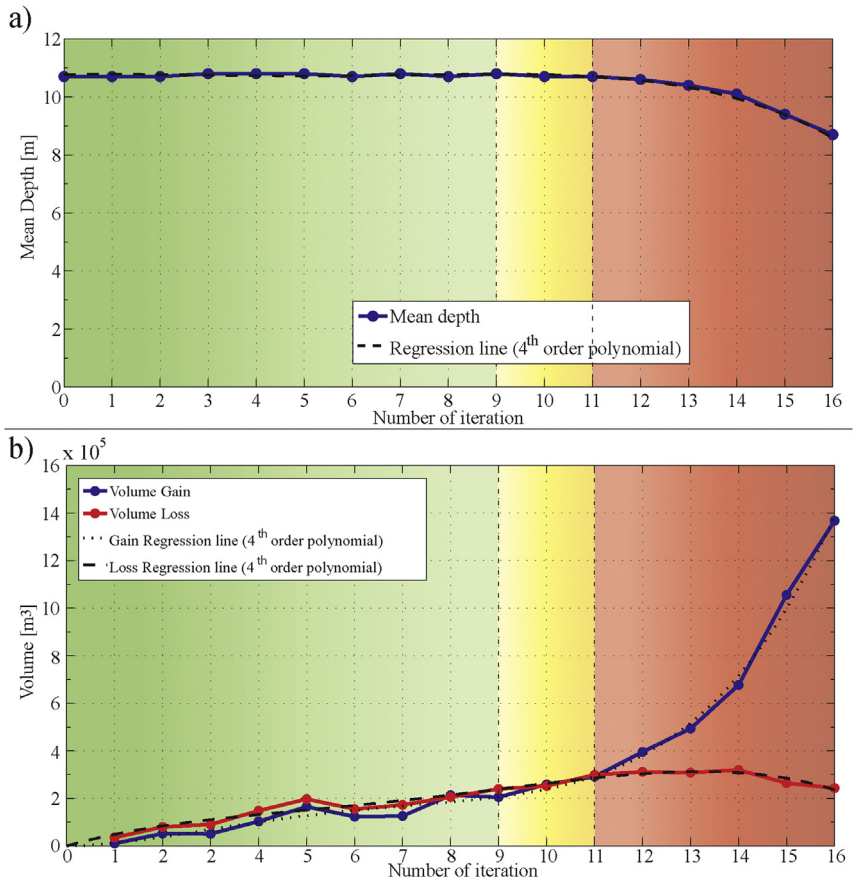

Fig. 10. Graphs of the mean depths of all 17 maps created (a) and of volume differences between the total depth map and other maps from the 16 iterations (b) of the CL. Green and red colours in the background denote increasing differences between iterations. Dark green areas denote close similarities between the resulting maps; light to dark yellow areas and light to dark red areas denote similar decreases. (For interpretation of the references to colour in this figure legend, the reader is referred to the web version of this article.)

they show minor differences in geometry from the total and the 10th iteration. However, the profile of the surface reconstructed from the 16th iteration subset is considerably different in all the three sections.

Profile AA′ shows that differences from the 16th step surface are more pronounced in the upper and lower sections of the landslide and likely due to globally inhomogeneous point distributions in these areas that are often inaccessible due to the presence of private property or dense vegetation. In contrast, differences in the central part of the landslide are considerably reduced because the area is occupied by a village and farmland crossed by accessible roads, making it possible to perform a survey with more homogeneous point coverage. Analogous behaviour can be observed in marginal areas of the landslide that are characterized by inaccessible areas and are thus less surveyed. As a whole, the three proposed approaches substantially confirm the same hypothesis that differences between the resulting depth maps are minimal when using more than 50 measurements (as long as they are well distributed). In other words, to generate an approximate representation of the slip surface depth of the CL, a minimum number of 39 H/V single stations must be used. Increasing the number of measures to 49 considerably enhances the accuracy and reliability of the model, but using more than 60 measurement points generates moderate improvements in model quality.

5.1.2. Roccalbegna landslide case study

Plots of the average depth values and volumetric differences are shown in Fig. 12. The plot of the mean depth (Fig. 12a) reveals minor variations for the first 13 iterations. From the 17th iteration onward, the graph shows a considerable increase in gradients, denoting a more significant difference between the resulting maps. The mean depth calculated for maps corresponding to the first 13 iterations consistently ranges from 11.28 m to 11.90 m with an average value of 11.56 m and a standard deviation equal to 0.2 m (dark to light green areas in Fig. 12a); in the maps of successive iterations, values decrease considerably up to a value of 8.73 m due to the insufficient spatial density of measurements made (yellow to red areas in Fig. 12a). The graph of volume differences shows the same gradual increase in both areas with volume gains and losses occurring until the 13th step (green areas in Fig. 12b). From the 13th and 17th iterations onward, the two series continue to exhibit similar trends but with a slight gradual increase in gradients (light to dark yellow areas in Fig. 12b). From the 17th iteration onward, the two series show completely different behaviour as shown for the CL, tending to diverge (light to dark red areas in Fig. 12a). In particular, the series of volume gains denotes exponential behaviour while the series of volume loss shows a declining gradient until the 17th iteration, where it starts to decrease. This behaviour is analogous to that observed for Castagnola, where an insufficient number and spatial density of measurement points render calculated surfaces progressively more inaccurate and decreasing in depth.

Fig. 13a shows the differences in depth between the map obtained from all of the data and that obtained using data of the 22nd iteration for the profiles of sections AA′, BB′ and CC′ (Fig. 13b–d, respectively). The profiles were calculated using depth maps from the total dataset and from the 10th and 22nd iterations, and they

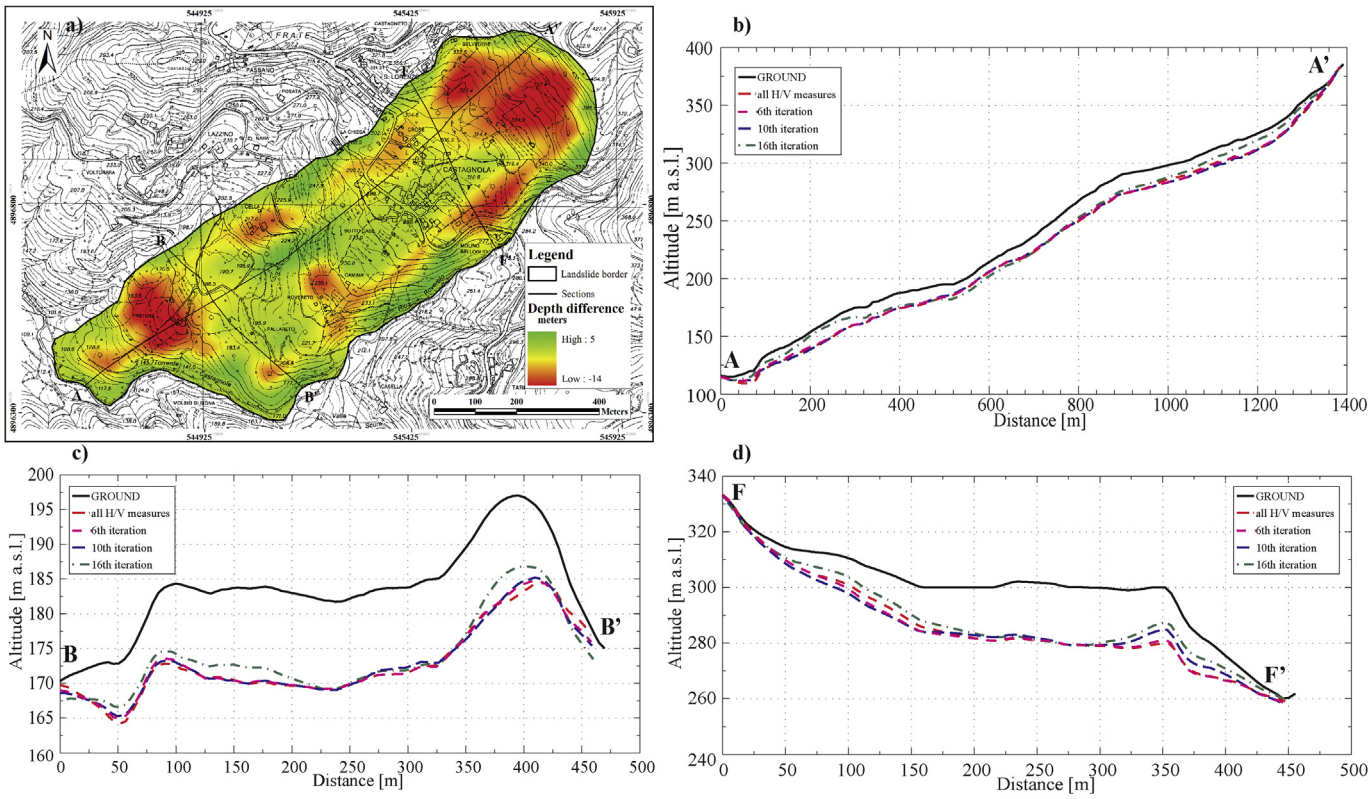

Fig. 11. Map of differences in depth between the slip surface obtained using all of the data and that obtained using data from the 16th iteration. The four height profiles show the ground topography and slip surfaces obtained using all of the data and data from the 6th, 10th and 16th iterations in correspondence with sections AA′, BB′ and FF′, respectively.

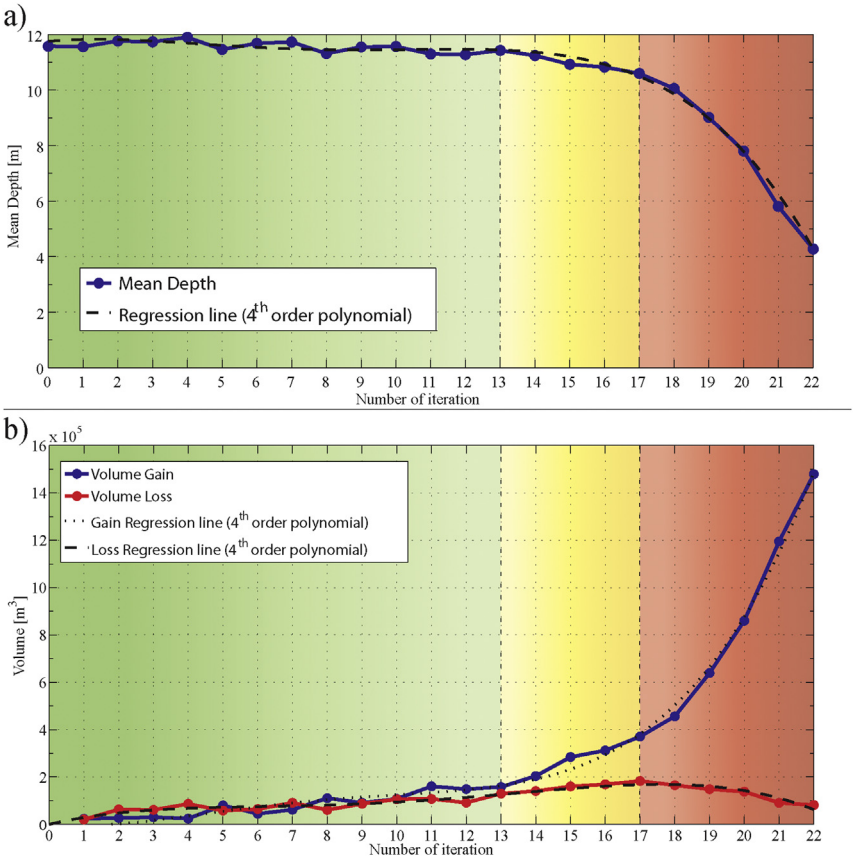

Fig. 12. Graphs of the mean depths of all 23 calculated maps (a) and of volume differences between the total depth map and other maps from the 22 iterations (b) of RL. Green and red coloured areas in the background denote increasing differences between the iterations. Dark green areas denote close similarities between the resulting maps; light to dark yellow areas and light to dark red areas denote similar decreases. (For interpretation of the references to colour in this figure legend, the reader is referred to the web version of this article.)

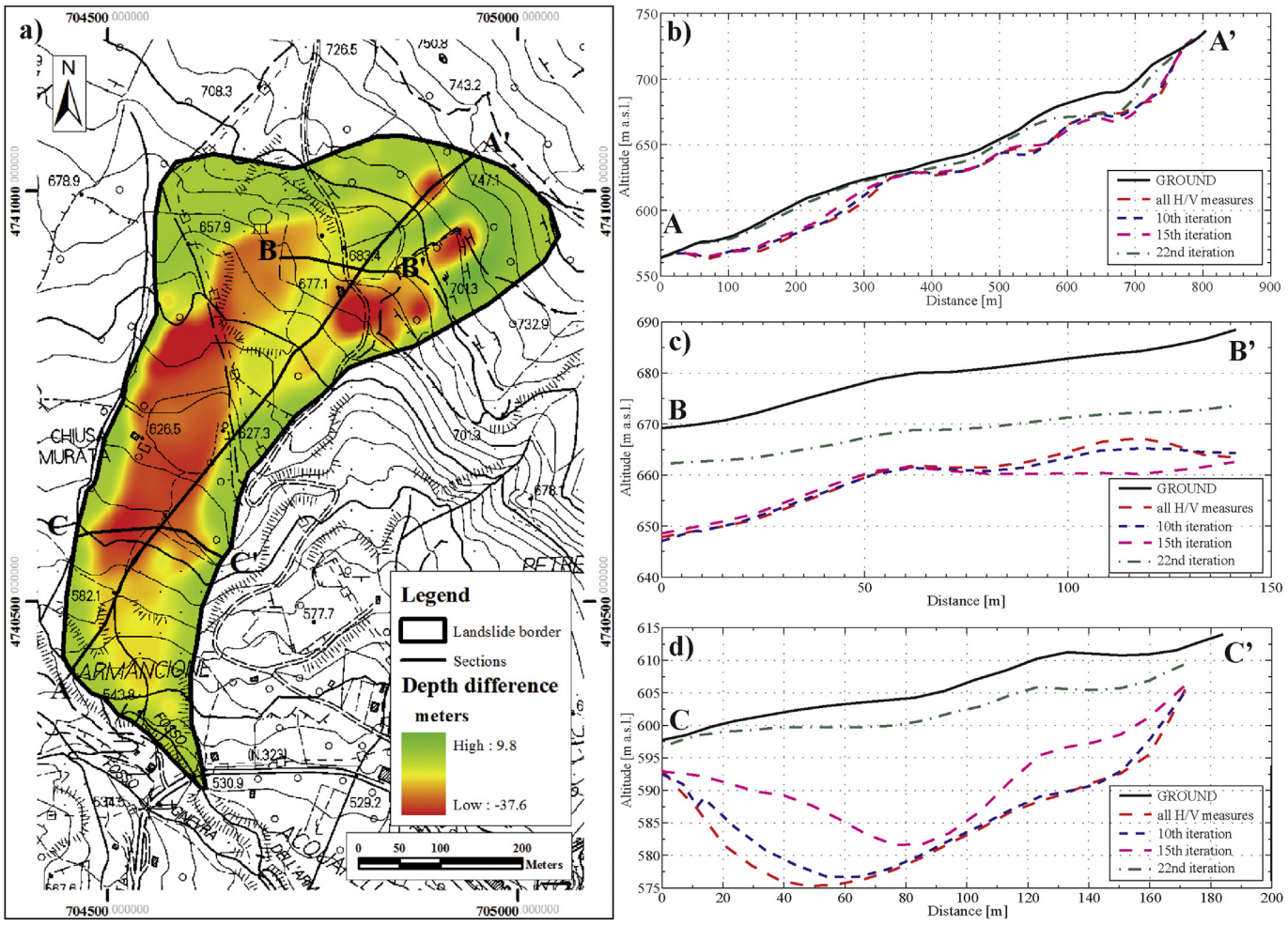

Fig. 13. Map of differences in depth between slip surfaces obtained using all of the data and that obtained from data of the 22nd iteration. The four height profiles show ground topographies and slip surfaces obtained from all of the data and fro data of the 10th, 15th and 22nd iterations in correspondence with sections AA′, BB′ and CC′, respectively.

show minor differences in geometry until the 10th iteration while the profile of the surface reconstructed using the 22nd subset shows considerably different results for all three sections.

As a whole, the three proposed approaches confirm that differences between the resulting depth maps are minor when applying more than 33–35 measurements (as long as they are well distributed). In other words, to provide an approximate representation of the slip surface depth of the RL, a minimum of 33 H/V single stations must be used. Increasing the number of measures used to 53 considerably enhances the accuracy and reliability of the model, and using more than 53 measurement points produces moderate improvements in model quality.

In conclusion, our approach based on the iterative reduction of an initial H/V measurement dataset provided a good evaluation of the quality of resulting depth maps. In addition, the approach serves as a valid tool for estimating the expected timing, costs and quality of seismic surveys on landslides based on the planned measurement quantity and density levels. Because the total number of measurements made per day is dependent on available instruments and because 20/30 measures per day can serve as a realistic parameter, the results of this work can facilitate an estimate of budgets required in terms of the timing and financial costs of efficient and accurate landslide slip surface detection.

However, it is necessary to note two main drawbacks of the proposed methodology: a) the contributions of topography were not considered during interpolation, and b) the initial datasets for both landslides were affected by an irregular spatial distribution mainly resulting from the presence of inaccessible areas and rugged terrain. In particular, our reconstruction of the depth map of Roccalbegna, for which numerous measures were represented in clusters due to the varying project requirements, was extensively affected by the total absence of measurement points in the northwestern part of the landslide area, thereby generating a biased estimation of a broad area where depth values of the slip surface are equal to zero. Finally, the use of pre-landslide DEM data could constitute an advantage rather than a drawback, as these are typically the only data available on the first day of an emergency.

6. Conclusions

Because slope instabilities are some of the more complex and dangerous phenomena that affect human life and activity, understanding internal structures of landslides can facilitate the execution of reliable stability analyses and, consequently, the adoption of mitigation procedures. The approach developed and discussed in this paper allows one to obtain, over a relatively short period of time, information of interest that can ultimately be used to plan the quantity and location of direct measurements (i.e., boreholes, inclinometers, and piezometers). Indeed, the use of H/V measurements generates timely information on the main impedance contrast depths for large areas over a few days at relatively low costs. The interpolation of these timely depth

measures allows one to reliably detect and reconstruct landslide slip surfaces. The proposed approach was validated for the CL, for which direct measures of the subsoil are available. It was then applied to another case study of the RL, for which direct measurements apart from those of shallow soil layers, were not available.

These experiments conducted on the CL and RL serve as a proof of the opportunities that this approach can offer. To assess the accuracy of reconstructed seismic impedance contrasts associated with slip surfaces, an interpolation workflow was iterated by decreasing the number of H/V single stations involved in the reconstruction of slip surfaces. As a result, the following were determined: i) the minimum number of measurements for a homogeneous spatial distribution that ensures reliable reconstruction, ii) the range of measurements needed to considerably enhance the accuracy and reliability of the model and iii) the threshold number above which only slight improvements in model quality are expected.

The main drawbacks of this procedure are as follows: i) the seismic response of a landslide can be strongly affected by slope properties and shapes (e.g., geological features, physical properties, angle slopes, and impedance differences between the landslide mass and bedrock); ii) in the same landslide, seismic responses could vary, moving from one area to another (e.g., evidence of seismic amplification can disappear and seismic noise signals can be polarized, affecting the directionality of the signal itself); iii) the presence of inaccessible areas leads to an irregular spatial distribution of H/V measurements; and iv) artefacts resulting from rough topography. Through our two case studies, the reliability of the applied techniques was justified because topographic amplification/deamplification effects can be neglected with respect to landslide mass resonance, as the angle slope is less than 15°.

Furthermore, 2-D and 3-D numerical modelling methods designed to assess slope stability and perform back-analysis simulations have been developed in recent years to predict the behaviours of unstable slopes and their response to triggers (e.g., seismic shaking or rainfall). Nevertheless, such models still require access to detailed knowledge of the geological, mechanical, hydrological properties of landslides and boundary conditions. Therefore, the proposed methodology, in providing the depths of sliding surfaces and lateral geometries of landslide mass, is expected to constrain engineering-geological models, optimize the stability analysis outputs and stabilization plans, and ultimately reveal the best landslide mitigation procedures.

Acknowledgements

The authors would thank everyone who assisted them during the data collection period and local authorities for providing information. The authors are also grateful to the anonymous reviewers and to Guest Editor Dr. S. D'Amico for providing comments and improving the manuscript.

References

Abbate, E., Bortolotti, V., Principi, G., 1980. Apennine ophiolites: a peculiar oceanic crust. Ofioliti 1, 59–96.

Amoozegar, A., 1989. Compact constant head permeameter for measuring saturated hydraulic conductivity of the vadose zone. Soil Sci. Soc. Am. J. 53, 1356–1361.

Amorosi, A., Castellaro, S., Mulargia, F., 2008. Single-Station Passive Seismic Stratigraphy: an inexpensive tool for quick subsurface investigation. GeoActa 7, 29–39.

Antolini, F., Tofani, V., Del Ventisette, C., Luzi, G., Casagli, N., Moretti, S., 2013. SAR Interferometry for landslides risk assessment at local scale: the case study of Castagnola (Northern Apennines, Italy). In: Margottini, Claudio, et al. (Eds.), Landslide Science and Practice. Volume 2: Early Warning, Instrumentation and Monitoring. Springer Berlin Heidelberg, pp. 407–414.

Bicocchi, G., D'Ambrosio, M., Vannocci, P., Nocentini, M., Tacconi Stefanelli, C., Masi, E.B., Carnicelli, S., Tofani, V., Catani, F., 2015. Preliminary assessment of the factors controlling the geotechnical and hydrological properties in the hillslope deposits of eastern Tuscany (Central Italy). In: IAMG 2015 Proceedings, pp. 867–874. ISBN 978 3-00 050337 5.

Bicocchi, G., D'Ambrosio, M., Rossi, G., Rosi, A., Tacconi Stefanelli, C., Segoni, S., Nocentini, M., Vannocci, P., Tofani, V., Casagli, N., Catani, F., 2016. Shear strength and permeability in situ measures to improve landslide forecasting models: a case study in the Eastern Tuscany (Central Italy). In: Landslides and Engineered Slopes. Experience, Theory and Practice, pp. 419–424. http://dx.doi.org/10.1201/b21520-42.

Boccaletti, M., Guazzone, G., 1974. Remnant arcs and marginal basins in the Cenozoic development of the Mediterranean. Nature 252, 18–21.

Bonnefoy-Claudet, S., Cotton, F., Bard, P.Y., 2006. The nature of noise wavefield and its applications for site effects studies. A literature review. Earth Sci. Rev. 79, 205–227.

Bortolotti, V., Principi, G., Treves, B., 2001. Ophiolites, Ligurides and the tectonic evolution from spreading to convergence of a Mesozoic Western Tethys segment. In: Martini, I.P., Vai, G.B. (Eds.), Anatomy of an Orogen: the Apennines and Adjacent Mediterranean Basins. Kluwer Acad. Publ., Dordrecht, pp. 151–164.

Bouckovalas, G.D., Papadimitriou, A.G., 2005. Numerical evaluation of slope topography effects on seismic ground motion. Soil Dyn. Earthq. Eng. 25, 547–558. http://dx.doi.org/10.1016/j.soildyn.2004.11.008.

Bourdeau, C., Havenith, H.-B., 2008. Site effects modelling applied to slope affected by Suusamyr earthquake (Kyrgyzstan, 1992). Eng. Geol. 97, 126–145. http://dx.doi.org/10.1016/j.enggeo.2007.12.009.

Bozzano, F., Lenti, L., Martino, S., Paciello, A., Scarascia Mugnozza, G., 2011. Evidences of landslide earthquacke triggering due to self-excitation process. Int. J. Earth Sci. 100, 861–879.

Cartiel, R., Barazza, F., Pascolo, P., 2006. Improvement of Nakamura technique by singular spectrum analysis. Soil Dyn. Earthq. Eng. 26, 55–63.

Castellaro, S., Mulargia, F., Bianconi, L., 2005. Passive Seismic Stratigraphy: a new efficient, fast and economic technique. J. Geotech. Environ. Geol. 3, 51–77.

Castellaro, S., Mulargia, F., 2009a. The effect of velocity inversions on H/V. Pure Appl. Geophys. 166, 567–592.

Castellaro, S., Mulargia, F., 2009b. Vs30 estimates using constrained H/V measurements. Bull. Seismol. Soc. Am. 99, 761–773.

Cestari, G., Crescenzi, S., Montali, P., Orlandini, G., Spagna, V., 1979. Deformazione di versante e movimenti franosi nella parte alta dei bacini dei fiumi Albegna e Fiora (Toscana Meridionale). Esame dell'area campione del versante del M. Labbro. Geol. Appl. Idrogeol. 14 (2), 207–227.

Cruden, D.M., Varnes, D.J., 1996. Landslide types and processes. Landslides Invest.n Mitig. 247, 36–75.

Danneels, G., Bourdeau, C., Torgoev, I., Havenith, H.-B., 2008. Geophysical investigation and dynamic modelling of unstable slopes: case-study of Kainama (Kyrgyzstan). Geophys. J. Int. 175, 17–34. http://dx.doi.org/10.1111/j.1365-246X.2008.03873.x.

Decandia, F.A., Elter, P., 1972. La "zona" ofiolitifera del Bracco nel settore compreso tra Levanto e la Val Graveglia (Appennino Ligure). Mem. Soc. Geol. It 11 (Suppl. l.), 503–530.

Del Gaudio, V., Coccia, S., Wasowski, J., Gallipoli, M.R., Mucciarelli, M., 2008. Detection of directivity in seismic site response from microtremor spectral analysis. Nat. Hazards Earth Syst. Sci. 8, 751–762.

Delgado, J., Lopez Casado, C., Giner, J., Estévez, A., Cuenca, A., Molina, S., 2000. Microtremors as geophysical exploration tool: applications and limitations. Pure Appl. Geophys. 15, 1445–1462.

Delgado, J., Garrido, J., Lenti, L., Lopez-Casado, C., Martino, S., Sierra, F.J., 2015. Unconventional pseudostatic stability analysis of the Diezma landslide (Granada, Spain) based on a high-resolution engineering-geological model. Eng. Geol. 184, 81–95.

Del Gaudio, V., Muscillo, S., Wasowski, J., 2014. What we can learn about slope response to earthquake from ambient noise analysis: an overview. Eng. Geol. 182, 182–200. http://dx.doi.org/10.1016/j.enggeo.2014.05.010.

Del Soldato, M., Segoni, S., De Vita, P., Pazzi, V., Tofani, V., Moretti, S., 2016. Thickness model of pyroclastic soils along mountain slopes of Campania (southern Italy). In: Aversa, et al. (Eds.), Landslides and Engineered Slopes. Experience, Theory and Practice. Associazione GEotecnica Italaian, Rome, Italy, pp. 797–804. ISBN: 978-1-138-02988-0.

Elter, P., Giglia, G., Tongiorgi, M., Trevisan, L., 1975. Tensional and compressional areas in the recent (Tortonian to present) evolution of the Northern Apennines. Boll. Geofis. Teor. Appl. 42, 3–18.

Fäh, D., Kind, F., Giardini, D., 2001. A theoretical investigation of average H/V ratios. Geophys. J. Int. 145, 535–549.

Fidolini, F., Pazzi, V., Frodella, W., Morelli, S., Fanti, R., 2015. Geomorphological characterization, monitoring and modeling of the Monte Rotolon complex landslide (Recoaro Terme, Italy). In: Lollino, Giorgio, et al. (Eds.), Engineering Geology for Society and Territory – Volume 2: Landslide Processes. Springer International Publishing Switzerland.

Field, E.H., Jacob, K., 1993. The theoretical response of sedimentary layers to ambient seismic noise. Geophys. Res. Lett. 20–24, 2925–2928.

Frodella, W., Fidolini, F., Morelli, S., Pazzi, V., 2015. Application of infrared thermography for landslide mapping: the Rotolon DSGDS case study. Rendiconti Online della Soc. Geol. Ital. XX, 144–147. http://dx.doi.org/10.3301/ROL.2015.85.

Galea, P., D'Amico, S., Farrugia, D., 2014. Dynamic characteristics of an active coastal spreading area using ambient noise measurements – (Anchor Bay, Malta). Geophys. J. Int. 199, 1166–1175. http://dx.doi.org/10.1093/gji/ggu318.
Hack, R., 2000. Geophysics for slope stability. Surv. Geophys. 21, 423–448.
Herak, M., 2008. The use of ambient noise for buildind and soil characterization. In: Mucciarelli, M., Herak, M., Cassidy, J. (Eds.), Increasing Seismic Safety by Combining Engineering Technologies and Seismological Data, NATO Science for Peace and Security, Series C: Environmental Security ISSN1874-6519. Springer, Netherlands, pp. 1–138.
Ibs-Von Seht, M., Wohlenberg, J., 1999. Microtremor measurements used to map thickness of soft sediments. Bull. Seismol. Soc. Am. 89, 250–259.
Imposa, S., Fazio, F., Grassi, S., Cino, P., Rannisi, G., 2015. Geophysical surveys to study a landslide body (North-Eastern Sicily). In: Proceeding of the International Conference: Geo-Risks in Mediterranean and their 651 mitigation. 20-21 July. University of Malta.
Jacobacci, A., Martelli, G., Nappi, G., 1967. In: Note Illustrative Della Carta Geologica D'Italia, Foglio 129 S. Fiora, Roma, p. 61.
Jongmans, D., Garambois, S., 2007. Geophysical investigation of landslides: a rewiev. Bull. Société Géologique Fr. 178, 101–112. http://dx.doi.org/10.2113/gssgfbull.178.2.101.
Konno, K., Ohmachi, T., 1998. Ground-motion characteristics estimated from spectral ratio between horizontal and vertical components of microtremor. Bull. Seismol. Soc. Am. 88, 228–241.
Lachet, C., Bard, P.Y., 1994. Numerical and theoretical investigations on the possibilities and limitation of Nakamura's technique. J. Phys. Earth 42, 377–397.
Lagormarsino, R., 2002. Chiese, cappelle, oratori della Valle di Deiva. In Santa Maria di Piazza. Culto, Territ. Pop. al crocevia una chiesa millenarian. In: I Quaderni della Tigullia, n. 2. Chiavari.
Lane, J.W., White, E.A., Steele, G.V., Cannia, J.C., 2008. Estimation of bedrock depth using the horizontal-to-vertical (H/V) ambient-noise seismic method. In: 21st EEGS Symposium on the Application of Geophysics to Engineering and Environmental Problems, pp. 490–502.
Larose, E., Carrière, S., Voisin, C., Bottelin, P., Baillet, L., Guéguen, P., Walter, F., Jongmans, D., Guillier, B., Garambois, S., Gimbert, F., Massey, C., 2015. Environmental seismology: what can we learn on earth surface processes with ambient noise? J. Appl. Geophys. 116, 62–74. http://dx.doi.org/10.1016/j.appgeo.2015.02.001.
Lenti, L., Martino, S., 2012. The interaction of seismic waves with step-like slopes and its influence on landslide movements. Eng. Geol. 126, 19–36. http://dx.doi.org/10.1016/j.enggeo.2011.12.002.
Lermo, J., Chavez-Garcia, F.J., 1993. Site effect evaluation using spectral ratios with only one station. Bull. Seismol. Soc. Am. 83, 1574–1594.
Lermo, J., Chavez-Garcia, J., 1994. Are microtremors useful in site response evaluation? Bull. Seismol. Soc. Am. 84, 1350–1364.
Lotti, A., Saccorotti, G., Fiaschi, A., Matassoni, L., Gigli, G., Pazzi, V., Casagli, N., 2015. Seismic monitoring of rockslide: the torgiovannetto quarry (central Apennines, Italy). In: Lollino, G., et al. (Eds.), –, Engineering Geology for Society and Territory, vol. 2. Springer International Publishing, Switzerland, pp. 1537–1540. http://dx.doi.org/10.1007/978-3-319-09057-3_272.
Luttenegger, J.A., Hallberg, B.R., 1981. Borehole shear test in geotechnical investigations. Am. Soc. Test. Mater. Special Publ. 740, 566–578.
Maurer, H., Spillmann, T., Heincke, B., Hauck, C., Loew, S., Springman, S.M., Green, A.G., 2010. Geophysical characterization of slope instabilities. First break 28, 53–61.
Méric, O., Garamboise, S., Malet, J.P., Cadet, H., Guéguen, P., Jongmans, D., 2007. Seismic noise-based methods for soft-rock landslide characterization. Bull. Société Géologique Fr. 178, 137–148.
Moisidi, M., Vallianatos, F., Kershaw, S., Collins, P., 2015. Seismic site characterization of the Kastelli (Kissamos) Basin in northwest Crete (Greece): assessments using ambient noise recordings. Bull. Earthq. Eng. 13, 725–753. http://dx.doi.org/10.1007/s10518-014-9647-4.
Moisidi, M., Vallianatos, F., Soupios, P., Kershaw, S., Rust, D., Piscitelli, S., 2012. Spatial spectral variations of microtremors and electrical resistivity tomography surveys for fault determination in southwestern Crete, Greece. J. Geophys. Eng. 9, 261–270.
Nakamura, Y., 1989. A method for dynamic characteristics estimation of subsurface using microtremor on the ground surface. Q. Rep. Railw. Tech. Res. Inst. 30, 25–33.
Nosengo, S., 1987. Scheda di Rilevamento delle situazioni di rischio idrogeologico, ai sensi del D.L. 30/06/1986 n. 309 compilata il 11 giugno 1987.
Okada, H., 2003. The microtremor survey methods. In: Geophysical Monography Series, vol. 12. Society of Exploration Geophysics.
Oliver, M.A., 1990. Kriging: a method of interpolation for geographical information systems. Int. J. Geogr. Inf. Syst. 4, 313–332.
Panzera, F., D'Amico, S., Lotteri, A., Galea, P., Lombardo, G., 2012. Seismic site response of unstable steep slope using noise measurements: the case study of Xemxija bay area, Malta. Nat. Hazard Earth Sci. Syst. 12, 3421–3431. http://dx.doi.org/10.5194/nhess-12-3421-2012.
Pazzi, V., Morelli, S., Fidolini, F., Krymi, E., Casagli, N., Fanti, R., 2016a. Testing cost-effective methodologies for flood and seismic vulnerability assessment in communities of developing countries (Dajç northern Albania). Geomatics. Nat. Hazards Risk 7, 971–999. http://dx.doi.org/10.1080/19475705.2015.1004374.
Pazzi, V., Morelli, S., Pratesi, F., Sodi, T., Valori, L., Gambacciani, L., Casagli, N., 2016b. Assessing the safety of schools affected by geo-hydrologic hazards: the geo-hazard safety classification (GSC). Int. J. Disaster Risk Reduct. 15, 80–93.
Philip, J.R., 1985. Approximate analysis of the borehole permeameter in unsaturated soil. Water Resour. Res. 21, 1025–1033.
SESAME, 2004. Guidelines for the implementation of the H/V spectral ratio technique on ambient vibrations. Measurements, processing and interpretation. In: SESAME European Research Project, WP12 – Deliverable D23.12, European Commission – Research General Directorate. Project No. EVG1-CT-2000–00026 SESAME.
Shepard, D., 1968. A two-dimensional interpolation function for irregularly-spaced data. In: Proceedings of 23rd National Conference A.C.M.: 517–524.
Spizzichino, D., Margottini, C., Castellaro, S., Mulargia, F., 2013. Passive seismic survey for cultural heritage landslide risk assessment. In: Margottini, Claudio, et al. (Eds.), Landslide Science and Practice. Volume 6: Risk Assessment, Management and Mitigation. Springer Berlin Heidelberg, pp. 483–489.
Tofani, V., Del Ventisette, C., Moretti, S., Casagli, N., 2014. Integration of remote sensing techniques for intensity zonation within a landslide area: a case study in the northern Apennines, Italy. Remote Sens. 6 (2), 907–924.
Wang, L., Xu, Y., Xia, J., Luo, Y., 2015. Effect of near-surface topography on high-frequency Rayleigh-wave propagation. J. Appl. Geophys. 116, 93–103. http://dx.doi.org/10.1016/j.appgeo.2015.02.028.